Volume 14
Number 45
7 December 2022
Pages 16697-17082

Nanoscale

rsc.li/nanoscale

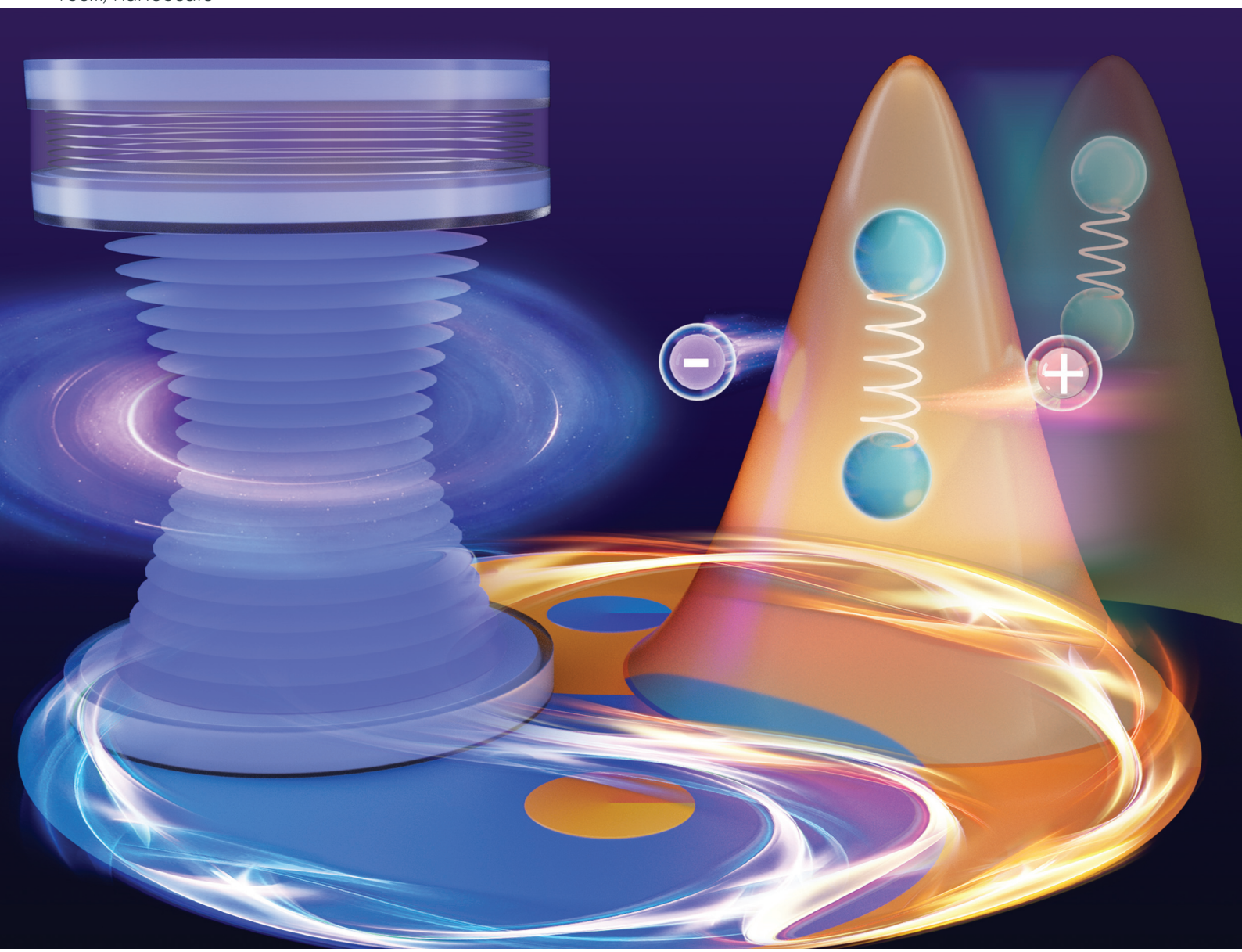

ISSN 2040-3372

ROYAL SOCIETY OF CHEMISTRY

REVIEW ARTICLE
Haonan Chang and Jun Zhang
From cavity optomechanics to cavity-less exciton optomechanics: a review

NCNST

Nanoscale

REVIEW

View Article Online
View Journal | View Issue

Cite this: *Nanoscale*, 2022, **14**, 16710

From cavity optomechanics to cavity-less exciton optomechanics: a review

Haonan Chang [a,b] and Jun Zhang *[a,b]

Cavity optomechanical coupling based on radiation pressure, photothermal forces and the photoelastic effect has been investigated widely over the past few decades, including optical measurements of mechanical vibration, dynamic backaction damping and amplification, nonlinear dynamics, quantum state transfer and so on. However, the delicate cavity operation, including cavity stabilization, fine detuning, tapered fibre access *etc.*, limits the integration of cavity optomechanical devices. Dynamic backaction damping and amplification based on cavity-less exciton optomechanical coupling in III–V semiconductor nanomechanical systems, semiconductor nanoribbons and monolayer transition metal dichalcogenides have been demonstrated in recent years. The cavity-less exciton optomechanical systems interconnect photons, phonons and excitons in a highly integrable platform, opening up the development of integrable optomechanics. Furthermore, the highly tunable exciton resonance enables the exciton optomechanical coupling strength to be tuned. In this review, the mechanisms of cavity optomechanical coupling, the principles of exciton optomechanical coupling and the recent progress of cavity-less exciton optomechanics are reviewed. Moreover, the perspectives for exciton optomechanical devices are described.

Received 11th July 2022,
Accepted 23rd September 2022

DOI: 10.1039/d2nr03784j

rsc.li/nanoscale

1. Introduction

The field of cavity optomechanics explores the interactions between electromagnetic waves and mechanical resonators.[1] Braginsky and his colleagues first experimentally demonstrated cavity optomechanical coupling *via* radiation pressure forces using a microwave cavity and revealed that the retarded

[a]*State Key Laboratory of Superlattices and Microstructures, Institute of Semiconductors, Chinese Academy of Sciences, Beijing 100083, China. E-mail: zhangjwill@semi.ac.cn*
[b]*Center of Materials Science and Optoelectronics Engineering, University of Chinese Academy of Sciences, Beijing 100049, China*

Haonan Chang

Haonan Chang is now a Master's student supervised by Prof. Jun Zhang in the State Key Laboratory of Superlattices and Microstructures, Institute of Semiconductors, Chinese Academy of Sciences. He received his Bachelor's degree from Beijing University of Posts and Telecommunications in China. His current research interest focuses on high-frequency cavity optomechanics and cavity-less exciton optomechanics.

Jun Zhang

Jun Zhang received a Bachelor's degree from Inner Mongolia University in China in 2004, and a Ph.D. from the Institute of Semiconductors, Chinese Academy of Sciences in 2010. Then he worked as a postdoctoral fellow at Nanyang Technological University in Singapore from 2010 to 2015 and joined the State Key Laboratory of Superlattices and Microstructures, Institute of Semiconductors, Chinese Academy of Sciences as a professor in 2015. His current research focuses on light–matter interactions in semiconductor materials, including Raman and Brillouin scattering, laser cooling in semiconductors, and quantum emitters in semiconductors.

nature of the force provides either damping or amplification of mechanical motion in 1967.[2] Dorsel *et al.* implemented the first cavity optomechanical experiment in the optical domain and demonstrated bistability of the radiation pressure force in 1983.[3] In 1993, J. Mertz *et al.* realized cavity optomechanical coupling based on the photothermal effect by imposing thermal stress on the cantilever using an auxiliary laser beam.[4] C. H. Metzger *et al.* exploited photothermal forces to suppress the Brownian vibrational fluctuations of a microlever from room temperature to an effective temperature of 18 K in 2004.[5] G. Bahl and colleagues reported cavity optomechanical coupling *via* a photoelastic effect and spontaneous Brillouin cooling in whispering-gallery cavity optomechanical systems in 2012.[6] In the following, we will review the field of cavity optomechanics based on these optomechanical coupling mechanisms.

In recent years, cavity optomechanics has attracted extensive attention, and has played an important role in a broad range of applications, such as phonon lasing[7–12] and damping,[5,13–20] telecommunications,[21–25] quantum information processing,[21,22,24,26] precise measurement and so on.[27–29] In the field of fundamental science, quantum effects of macroscopic objects can be observed through strong cavity optomechanical coupling[21–23,27,29–32] and cavity optomechanical systems are also an excellent platform for detecting gravitational waves.[33] In cavity optomechanical systems, various phenomena can be observed when the pump laser frequency is red-detuned or blue-detuned from the cavity resonance frequency. On the "heating" regime, *i.e.*, blue-detuning regime, where the pump laser frequency is lower than the cavity resonance frequency, coherent mechanical vibrations are excited through optical pumping, where phonon lasing and nonlinear optical effects, such as chaos,[34,35] solitons,[36] and surface acoustic wave frequency combs,[37,38] can be observed. On the "cooling" regime, *i.e.*, red-detuning regime, where the pump laser frequency is higher than the cavity resonance frequency, laser cooling[18–20] and state exchange between two resonant oscillators[21,39] can occur, which provides a toolbox for quantum communication protocols. Although the field of cavity optomechanics is prosperous, the abovementioned applications all require a delicate cavity operation, which is like the "sword of Damocles" for the integrated applications of optomechanics. Hence, alternative approaches are required in order to practically apply the optical control capability to integrated optomechanical systems. The "cavity-less" scheme is strongly desired to be developed.[42]

In recent years, some research groups have begun to explore the field of cavity-less optomechanics, such as exciton optomechanics. Yeo *et al.* and Montinaro *et al.* have reported the coupling of exciton and mechanical motion in quantum dot-nanowire hybrid systems.[40,41] Hajime Okamoto and his colleagues have reported exciton optomechanical coupling in III–V semiconductor heterojunction systems.[42,43] Jun Zhang *et al.* have reported laser cooling specific phonon modes in ZnTe nanoribbons *via* exciton optomechanical coupling.[44] H. Xie *et al.* have reported highly tunable exciton optomechanical coupling in the suspended monolayer $MoSe_2$.[45] Excitons are neutral quasiparticles, which are bound states of electrons and holes formed by Coulomb interactions.[46] The presence of strong exciton resonances in some semiconductors strongly interacts with incident pump lasers and presents an interesting platform to explore optomechanical effects without the need for an optical cavity.[45,47] To our knowledge, cavity-less exciton optomechanics has advantages as follows. First, cavity-less exciton optomechanics interconnects photons, phonons and excitons, which provides a new platform for fundamental studies in new regimes, where simultaneously strong optical and mechanical nonlinearity can be achieved.[45] Second, the optomechanical coupling rate is gate-tunable based on photothermal backaction in exciton optomechanical systems composed of two-dimensional semiconductor materials.[45] Third, the opto-piezoelectric backaction from the bound electron–hole pair enables us to probe excitonic transition simply with a sub-nanowatt power of light, realizing high-sensitivity optomechanical spectroscopy,[42] which would provide a novel way to improve the sensitivity of optomechanical sensing. Fourth, the exciton optomechanical system is a platform for ultrahigh-frequency mechanical resonators. The mechanical vibration in ref. 44 could reach 6.23 THz. Hence, cavity-less exciton optomechanics is a promising research field.

In this review, we will review the field of cavity optomechanics and cavity-less exciton optomechanics. In section 2, we will first introduce several mechanisms of cavity optomechanical coupling and the new research progress in cavity optomechanics based on the corresponding mechanisms. In section 3 we will introduce the fundamental principles involved in cavity-less exciton optomechanics, such as the excitation of excitons, exciton-mediated optomechanical forces, and the effect of strain on exciton resonance. In section 4, we will introduce the latest progress in the field of cavity-less exciton optomechanics and propose the future development direction of cavity-less exciton optomechanics.

2. Basic mechanisms of cavity optomechanical coupling

2.1. Radiation pressure

Light carries momentum, which leads to radiation pressure forces.[1] This force predicted by Maxwell was first discovered in experiments by P. N. Lebedev in 1900 and E. F. Nichols and G. F. Hull in 1901 using a light mill configuration in 1901.[48,116] In 1909, Einstein revealed the dual wave–particle nature of blackbody radiation by investigating radiation pressure force fluctuations acting on a movable mirror. Based on the above experiments, Frisch and Beth demonstrated that photons transfer momentum to atoms and macroscopic objects, respectively.[49,50] A typical Fabry–Perot cavity optomechanical coupling *via* a radiation pressure system is shown in Fig. 1(a). The cavity of length L consists of a stationary mirror and a moving mirror mounted on a spring. The optomechanical coupling principles in this system are introduced as

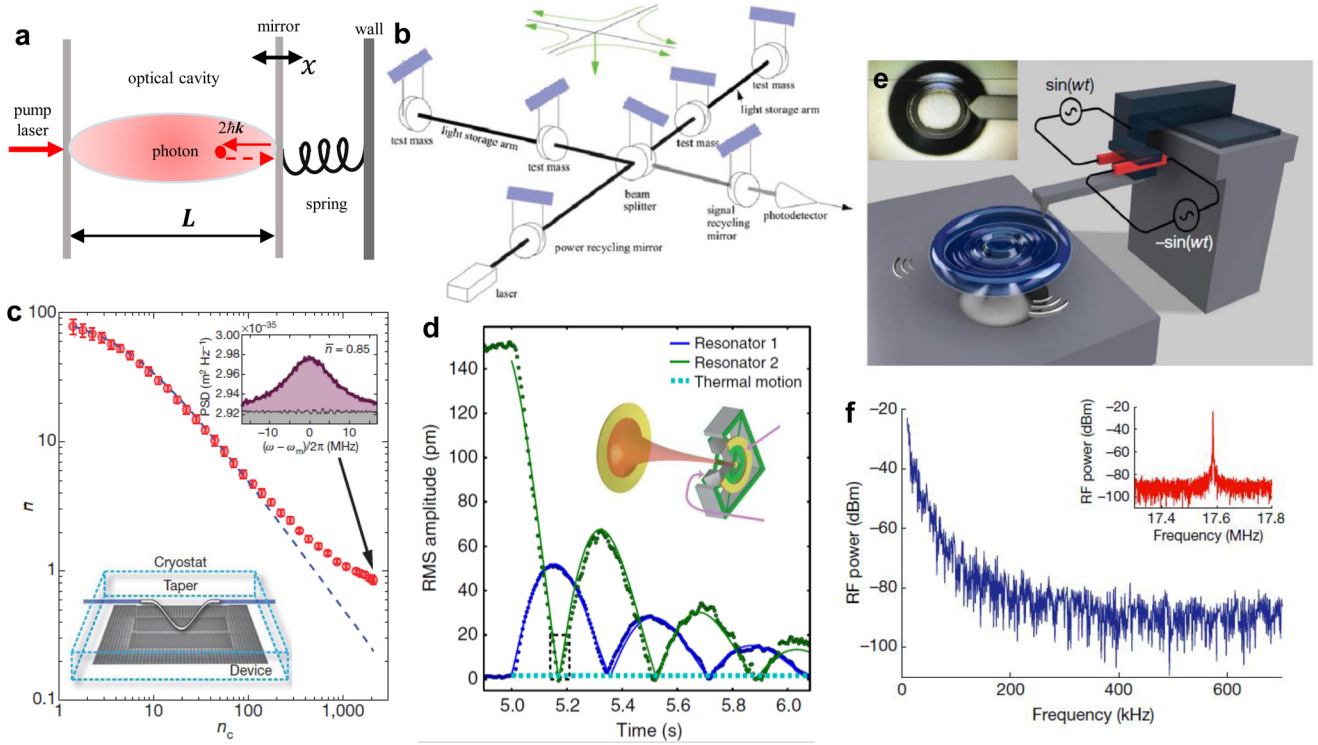

Fig. 1 Cavity optomechanical coupling *via* radiation pressure. (a) Schematic of the cavity optomechanical system, with a Fabry–Perot cavity of length L, with one mirror fixed and the other mounted on a spring. (b) Schematic of the gravitational wave detector LIGO. Reprinted with permission from ref. 33. Copyright 2018, American Physical Society. (c) Average phonon occupation number *versus* cooling drive-laser power. The bottom inset is the optomechanical device. Reprinted with permission from ref. 51. Copyright 2011, Nature. (d) A single swapping interaction shows phonon Rabi oscillations. The inset is an optical cavity coupled with two mechanical resonators. Reprinted with permission from ref. 52. Copyright 2017, Nature. (e) Experimental set-up for discovering optomechanical dissipative solitons. (f) Power spectrum of the mechanical mode in the solitons regime. Reprinted with permission from ref. 36. Copyright 2021, Nature.

follows. The photons with momentum $\boldsymbol{p} = \hbar\boldsymbol{k}$, where $\hbar$ is the reduced Planck's constant, reflected off the moving mirror transfer a momentum $2\hbar\boldsymbol{k}$ onto the mirror because of the laws of conservation of momentum. Due to the existence of the cavity, the number of intracavity photons increases. Hence, the interaction between the photons and the moving mirror is enhanced, which leads to the displacement of the moving mirror and a change of the cavity length L. The change of cavity length alters the cavity resonance frequency, which gives rise to detuning between the changed cavity resonance frequency and the unchanged frequency of the pump laser. The detuning determines the light amplitude inside the cavity, which subsequently leads to a change of the cavity length. Therefore, it creates a closed loop: the number of photons inside the cavity causes the radiation pressure force and the displacement of the mirror, and the radiation pressure force effectively depends on the mirror position.

The detuning frequency Δ is defined by $\Delta = \omega_0 - \omega_{\mathrm{cav}}$ and many different physical phenomena can be realized by changing the sign of Δ in the optomechanical system. In the resonant regime, *i.e.*, $\Delta = 0$, the cavity can be operated as an interferometer. The gravitational wave detector LIGO is shown in Fig. 1(b), which is a typical example although LIGO is dedicated to the detection of gravitational waves and not the investigation of optomechanics specifically.[33] The combination of the input and end test mass comprises Fabry–Perot cavities which can bounce the light between them many times (typically several hundred times) to increase the gravitational wave-induced sidebands by the number of bounces before returning the light to the beam splitter, which greatly improved measurement accuracy. In the red-detuning regime, *i.e.*, $\Delta < 0$, optomechanical laser cooling and state exchange between two resonant oscillators can occur. As shown in Fig. 1(c), J. Chan *et al.* reported that they used radiation pressure from a red-detuned laser ($\Delta = -\omega_{\mathrm{m}}$), where ω_{m} is the frequency of the mechanical resonator, to cool the mechanical motion down to its quantum ground state based on a coupled, nanoscale optical and mechanical resonator formed in a silicon microchip.[51] In this strong coupling regime, two resonant oscillators can exchange state between each other. As shown in Fig. 1(d), an optical cavity couples with two mechanical resonators and two incident laser beams are red-detuned from the cavity resonance frequency.[52] Optomechanical efficient coherent state swapping between two spatially and frequency separated mechanical resonators can be realized, which gives inspiration to investigate the quantum effects of many resonators. In blue-detuning

regime, *i.e.*, $\Delta > 0$, phonon lasing and nonlinear optomechanical effects can be realized. Jing Zhang *et al.* discovered dissipative solitons in the whispering-gallery cavity optomechanical systems. The experimental setup is shown in Fig. 1(e); when the phonon gain compensates the mechanical loss and optomechanical nonlinearity is balanced, stable localized mechanical wave packets coexisting with mechanical solitons can be realized (Fig. 1(f)), which provides a new toolbox for optomechanical applications.[36] In a word, cavity optomechanical system coupling *via* radiation pressure force is a promising platform for quantum coherent optomechanics.

2.2. Photothermal forces

Cavity optomechanical coupling *via* photothermal forces is another coupling mechanism.[53,54] The photothermal forces have been pointed out to be a significant source of force in optomechanical systems, competing with standard radiation pressure interactions. The basic coupling mechanism of photothermal forces compared with that of radiation pressure forces is shown in Fig. 2(a).[55] A Langevin-type force F^{L} imposed on the system induces a displacement δx in the mechanical position, which contributes to the optical resonance frequency shift $\delta\omega$, causing a delayed modulation in the number of intracavity photons δn. The top part of Fig. 2(a) depicts optomechanical backaction through radiation pressure forces F^{RP}. The bottom part depicts photothermal backaction through thermal stress F^{θ}. The specific process is as follows: the absorption of photons causes temperature fluctuations $\delta\theta$. The thermal stresses induced by the absorption process act back on the mechanical resonator, which leads to amplification or cooling of amplitude of the mechanical vibration. The expression of thermal stress F^{θ} is as follows:

$$F_n^{\theta}(t) = \frac{\partial}{\partial x_n}\int S^x : (c : S^{\theta})\mathrm{d}V = \int S_n^x : (c : S^{\theta})\mathrm{d}V, \qquad (1)$$

where S^x and S^{θ} are elastic and thermal strain stresses, respectively. The $x_n(t)$ is the normal mode amplitudes, the operator ":" denotes the tensor contraction operation and c is the stiffness tensor. This expression demonstrates the energy transferred between thermal and mechanical vibration. Hence, the above process forms a closed loop, which is so-called optomechanical coupling *via* thermal forces.[55]

The modulation of mechanical oscillators, including the cooling or amplification of mechanical resonators in various optomechanical systems, can be realized by time-delayed forces induced by a finite thermal and response time. Graphene is a two-dimensional material with low mass and stiffness, large thermal conductivity and high light absorption coefficient.[56–62] Due to the virtue of its low mass and stiffness,[63] which could improve the sensitivity of the optomechanical systems to the forces of light, it is an attractive candidate for mechanical resonators.[57,64–66] Besides, the large

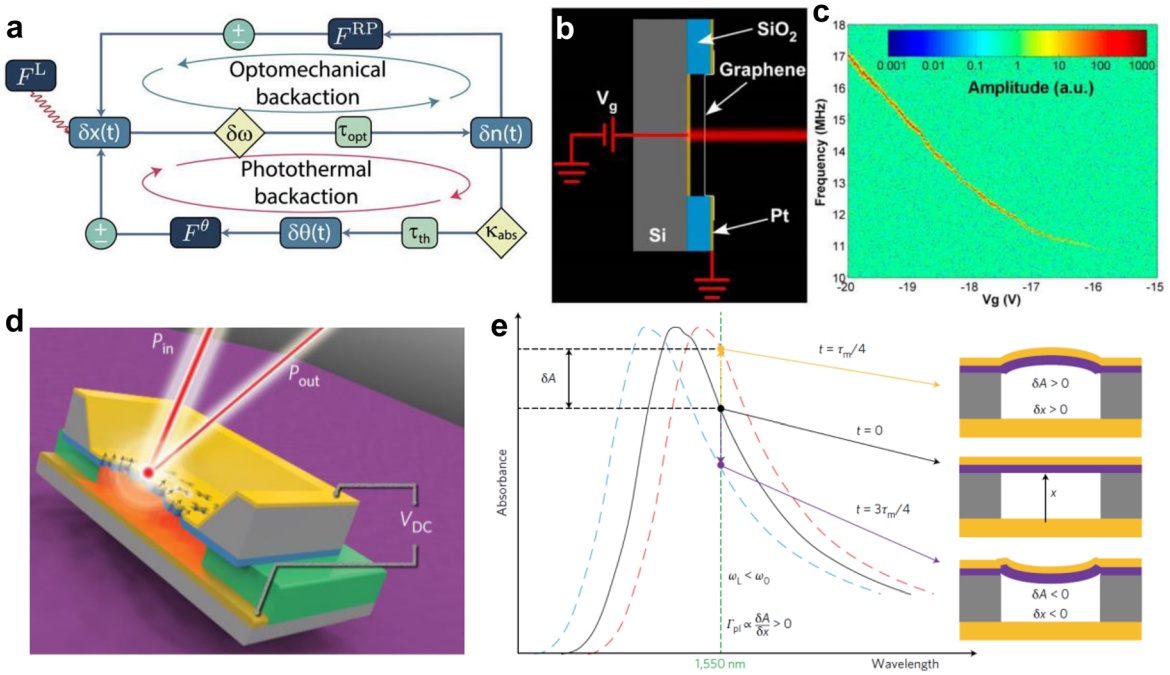

Fig. 2 Cavity optomechanical coupling *via* photothermal forces. (a) Schematic diagram of optomechanical coupling mechanisms based on photothermal forces and radiation pressure. Reprinted with permission from ref. 55. Copyright 2021, American Institute of Physics. (b) Experimental set-up of optomechanical devices based on graphene. (c) Photothermal self-oscillation of a graphene resonator. Reprinted with permission from ref. 70. Copyright 2012, American Chemical Society. (d) Schematic of the plasmomechanical Fano resonance device. The power of the incident laser beam is P_{in}, and P_{out} is the power of reflected light after interaction with the optomechanical device. (e) Plasmomechanical coupling. Left: Fano resonance of the optomechanical system. τ_m, period of mechanical resonance. δA, the optical absorption coefficient modulation. Right: Schematic of the bending of the bilayer membrane changing resonance frequency. Reprinted with permission from ref. 77. Copyright 2016, Nature.

thermal conductivity[67] and light absorption coefficient of graphene[68] demonstrate that graphene resonators are advantageous platforms to realize photothermal backaction and then enable laser cooling resonators to the quantum ground state.[69] A graphene-based cavity optomechanical structure is shown in Fig. 2(b).[70] The resonators are suspended monolayer graphene clamped on all sides to a silicon dioxide substrate with a source, drain, and gate electrodes, and the low finesse Fabry–Perot cavity consists of a graphene layer and platinum backplane. The voltage V_g is modulated for measurements of driven motion and tuning of the optical properties of the cavity. The vibration of graphene is actuated by voltage V_g between the graphene and the backplane. The displacement between the graphene and backplane could change the reflectivity R due to the change of optical cavity length. The feedback of this system comes from the fact that the motion of the membrane induces a force parallel to the velocity acting on the resonator with some time delay. Two possible candidates are photothermal forces and radiation pressure forces. According to the theoretical prediction, the photothermal gradient force ∇F_{pth} is given by

$$\nabla F_{\mathrm{pth}} = AP\frac{4\pi^2 a}{\lambda}\sin\theta_0 \sin^2\left(\frac{4\pi}{\lambda}(d - z_0)\right), \quad (2)$$

where λ is the wavelength of the pump laser, $\theta_0 = \theta(z_0)$ and z_0 is the initial displacement of the graphene resonators from the horizontal position. When $\theta_0 = 0$, the $\nabla F_{\mathrm{pth}} = 0$. The membrane must start with a nonzero displacement in order to experience optomechanical effects. Hence, a gate voltage V_g must be applied to the membrane to break the symmetry. According to the dependence of the optomechanical damping rate Γ_{OM} on the wavelength of laser λ and V_g, Robert A. Barton *et al.* concluded that photothermal backaction is dominant in this optomechanical system. Moreover, the radiation pressure force is too weak to affect either the resonant frequency or the damping of the graphene resonators. As shown in Fig. 2(c), the self-oscillation frequency of the system can be tuned by changing voltage V_g, which leads to many promising applications in photonics and signal processing.[59,71,72]

Photonic metamaterials are artificial optical materials that can convert optical energy to heat energy efficiently.[73–76] Hai Zhu *et al.* presented a plasmonic metamaterial absorber in a cavity optomechanical system.[77] The cavity optomechanical system consists of a 25 mm gold layer with cross-shaped plasmonic nanoslot antennas and a SiN layer on a metal back-reflector (Fig. 2(d)). The gold–SiN bilayer membrane forms a Fabry–Perot cavity. The hybridization of the cavity mode and plasmonic metamaterial resonance contributes to an optical Fano resonance, and the frequency of Fano resonance can be tuned by voltage V_{DC}. When incident light is absorbed by the gold nanoantenna layer, a strain is imposed on the bilayer membrane due to a thermoelastic process. Because of the different thermal expansion coefficient of gold and SiN, the bilayer membrane is bent by an out-of-plane displacement of δx and Fano resonance absorption is mechanically modulated by δA. They revealed that parameter $\delta A/\delta x$ is positive when the pump laser is red-detuned from Fano resonance and is negative when the pump laser is blue-detuned from Fano resonance. Due to the mechanical delayed response from the thermal heat flow, a force $F = -(\delta A/\delta x)v(t)$ is imposed on the mechanical resonator, where $v(t)$ is the speed of out-plane motion. When $\delta A/\delta x$ is positive, a mechanical resonance damping can be realized, *i.e.*, cooling a mechanical resonator. When $\delta A/\delta x$ is negative, mechanical vibration is amplified, which is an attractive candidate for a phonon laser.[78] This work paves a novel path to modifying the properties of optical cavities in cavity optomechanics *via* optical metamaterials.

2.3. Photoelastic interaction

For the photoelastic coupling cavity optomechanics, the feedback is obtained *via* inelastic scattering processes, including Raman scattering processes and Brillouin scattering processes.[79–81] Both Raman scattering and Brillouin scattering arise from the photoelastic scattering due to the density fluctuation of the medium.[82] For Brillouin scattering, the "density fluctuation" comes from stress waves (acoustic phonons). For Raman scattering, the "density fluctuation" comes from the relative displacement of oppositely charged atoms (optical phonons). In general scattering theory, the local density change of acoustic phonons and optical phonons has the same origin within the mechanism of photoelastic coupling where the optical susceptibility of materials depends on the density changes.[44] In this section, we mainly introduce photoelastic cavity optomechanical coupling in Brillouin scattering. Photoelastic optomechanical coupling *via* exciton resonance in Raman scattering will be introduced in the section 4.1.

The photoelastic cavity optomechanical coupling in whispering-gallery resonators *via* a Brillouin scattering process is shown in Fig. 3(a).[6] The Brillouin optomechanical process involves two optical whispering-gallery modes (OWGM), separated in the frequency space by the frequency of the acoustic whispering-gallery mode (AWGM) of interest. The model introduced is a forward scattering stimulated Brillouin scattering (SBS) setup, where the acoustic modes are low frequencies due to momentum conservation. The SBS process can be described as follows: the pump optical OWGM generates an AWGM *via* electrostrictive stress. The AWGM writes a traveling photoelastic grating that scatters light from the pump OWGM to the Stokes OWGM *via* a Brillouin scattering process.[83] At the same time, the electrostrictive interference pattern generated by the two OWGMs amplifies the acoustic WGM, which leads to positive feedback. The experimental setup on a silica microsphere resonator is shown in Fig. 3(b). A tapered optical fiber is employed to evanescently couple light into the pump OWGM. The pump OWGM is scattered by the AWGM and generates a Stokes OWGM. This scattered light and pump light also evanescently couple out to the tapered optical fiber and propagate to a photodetector at the opposite end of the fiber. The output pump laser and Stokes laser signals are shown in Fig. 3(c). The electrical beat signal (Fig. 3(d)) obtained from the photodetector provides the signature of the AWGM.

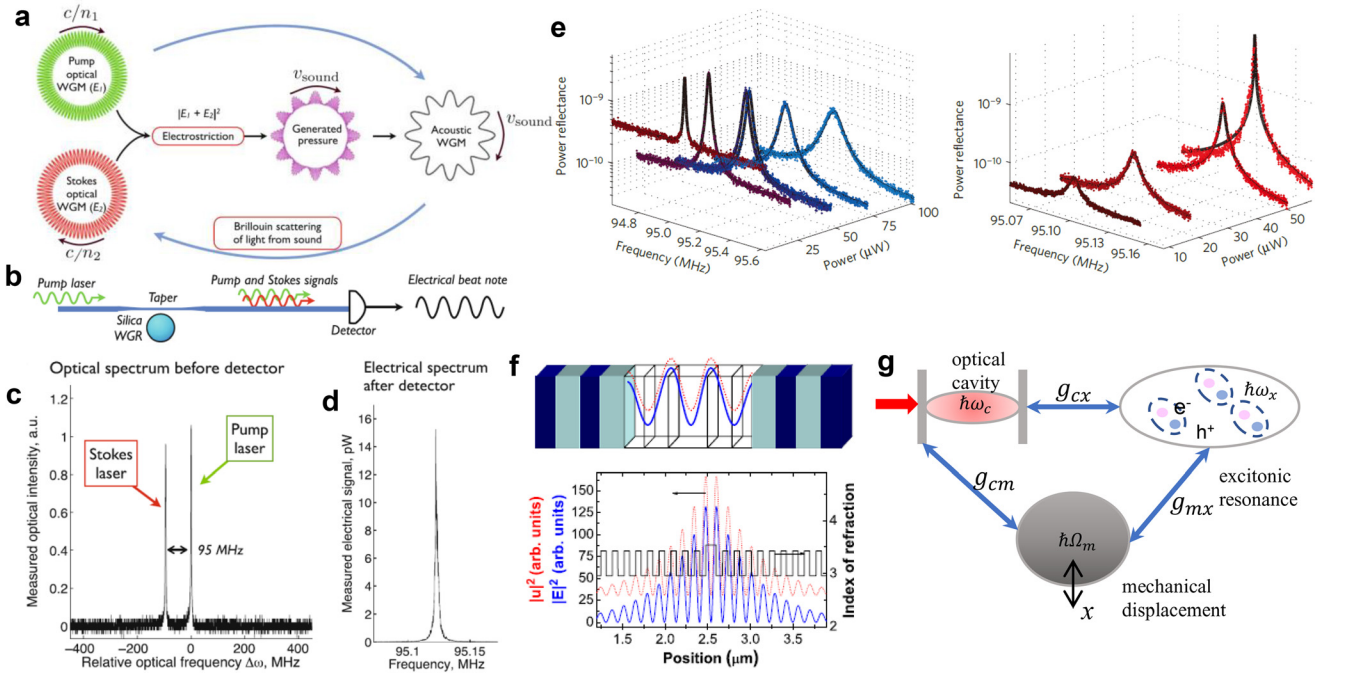

Fig. 3 Cavity optomechanical coupling *via* photoelastic interaction. (a) Optical whispering-gallery modes couple with acoustic whispering-gallery modes by a Brillouin scattering process. (b) Experimental setup. (c) Pump and Stokes laser at output. (d) An electrical beat signal provides acoustic eigenfrequency. Reprinted with permission from ref. 84. Copyright 2014, Springer. (e) Brillouin cooling (left panel) and heating (right panel) in whispering-gallery optomechanical devices. Reprinted with permission from ref. 6. Copyright 2012, Nature. (f) Ultrahigh-frequency cavity optomechanical devices with strong optomechanical coupling made of a GaAs/AlAs microcavity (up panel) and mechanical and optical eigenmodes (bottom panel). Reprinted with permission from ref. 89. Copyright 2012, American Physical Society. (g) Microcavity optomechanical coupling enhanced by exciton resonance.

There are two scattering mechanisms in Brillouin optomechanics: forward scattering and backward scattering. The backward Brillouin scattering is associated with large phonon momenta and therefore typically occurs with multi-GHz frequency acoustic waves. The forward Brillouin scattering in microcavities has allowed access to low-frequency acoustical modes where mechanical dissipation is lower than optical dissipation, in accordance with the requirements for cooling.[84] G. Bahl and his colleagues first observed a spontaneous Brillouin cooling low-frequency acoustic mode in the forward scattering whispering-gallery optomechanical system.[6] They broke the balance between the Stokes scattering and anti-Stokes scattering by optical resonance in the WGM, leading to a net absorption or generation of phonons by photons *via* photoelastic coupling. If the Stokes scattering is suppressed, cooling the acoustic mode would be realized (left panel in Fig. 3(e)). If anti-Stokes is suppressed, heating the acoustic mode would be realized (right panel in Fig. 3(e)). In this experiment, the photoelastic coefficient of the materials for photoelastic cavity optomechanical coupling is important. For some semiconductor materials, such as gallium arsenide,[85] the photoelastic coefficients are relatively larger than the photoelastic coefficients of silica,[86] and thus it is used as optomechanical resonators broadly.

Microcavity optomechanical devices based on a GaAs/AlAs structure are an outstanding candidate for ultrahigh-frequency optomechanical devices.[87,88,134] Because of a "double magic coincidence" of $Al_xGa_{1-x}As$,[89] the ratio between their acoustic and optical impedances as well as between their longitudinal acoustic phonon and photon propagation velocities are almost the same and independent of the composition x. The $Al_xGa_{1-x}As$ microcavity could confine photon and acoustic phonons of the same wavelength with a comparable quality factor Q. In 2013, A. Fainstein *et al.* reported that distributed Bragg reflector GaAs/AlAs vertical cavities could confine photons and phonons of the same wavelength and quality factor Q and realized strong optomechanical coupling, shown in Fig. 3(f).[89] Moreover, numerous pieces of literature have demonstrated a huge enhancement of optomechanical coupling between photons and GHz phonons in AlGaAs-based microcavities due to excitons (Fig. 3(g)).[127–130] The exciton is a neutral bound state of a hole and electron, which will be elaborated on in section 3.1. Alexander S. Kuznetsov and his colleagues introduced a novel platform for electrically driven exciton–polariton optomechanics at 20 GHz based on the coupling of polaritons and electrically generated bulk acoustic waves (BAWs) confined in an AlGaAs microcavity with QWs, in which the values of the Q_f product of the BAWs exceed 10^{14} Hz and the effective optomechanical coupling coefficient g_{eff} is around 50 THz nm^{-1}.[128] N. Carlon Zambon *et al.* theoretically investigated the case where the microcavity exciton optomechanical system operates in the strong exciton–photon coupling

regime.[131] The optical and excitonic resonances are parametrically modulated by the interaction with a mechanical mode and polariton–phonon interactions would enhance optomechanical coupling by two orders of magnitude. Besides, they analyzed that polariton nonlinearities affect dynamical backaction, modifying the capability to cool or amplify the mechanical motion.

2.4. Plasmon-molecule cavity optomechanics

In the abovementioned cavity optomechanical system, the interaction between photons and mechanical oscillators is introduced. In this section, the dynamical nature of the plasmon–molecule interaction will be introduced, which can be also demonstrated with the model of cavity optomechanics. A plasmon is a quantization of plasma oscillation,[91–93] which can be analogized with the energy quantum of the light field (photon) in cavity optomechanics. In the plasmon–molecule cavity optomechanical system (Fig. 4(a)), the mechanical resonator is molecule vibration. The optomechanical feedback loop of the plasmon–molecule cavity optomechanical system is shown in Fig. 4(c).[90] The plasmon force F_p with an amplification factor proportional to the time-averaged intracavity plasmonic field $\sqrt{\bar{n}_P}$ (induced by the pump laser) and to the Raman polarizability ($d\alpha/dx_v$), and thermal force F_{th} leads to the molecular displacement δx_v. As shown in Fig. 4(b), the molecular vibration changes the polarizability of the molecule, which in turn leads to a shift of the plasmon resonance frequency, closing the feedback looping. The Raman polarizability change induced by molecular vibration is the origin of the parametric optomechanical coupling. Surface enhanced Raman scattering (SERS), which was first reported by Fleischmann *et al.* in 1974, has enabled the detection of single molecules on the nanostructured surface.[94] However, there are no standard theoretical formalisms to interpret a number of experiment results of SERS. Philippe Roelli and his colleagues cited the concept of cavity optomechanics, regarded plasmons as photons in cavity optomechanics, and regarded molecular vibrations as phonons in cavity optomechanics.[90] Based on the model of cavity optomechanics, they successfully established a theoretical model of SERS and interpreted the dynamical nature of the plasmon–molecule interaction, making cavity optomechanics reach the molecular nanoscale.[95] Besides, the

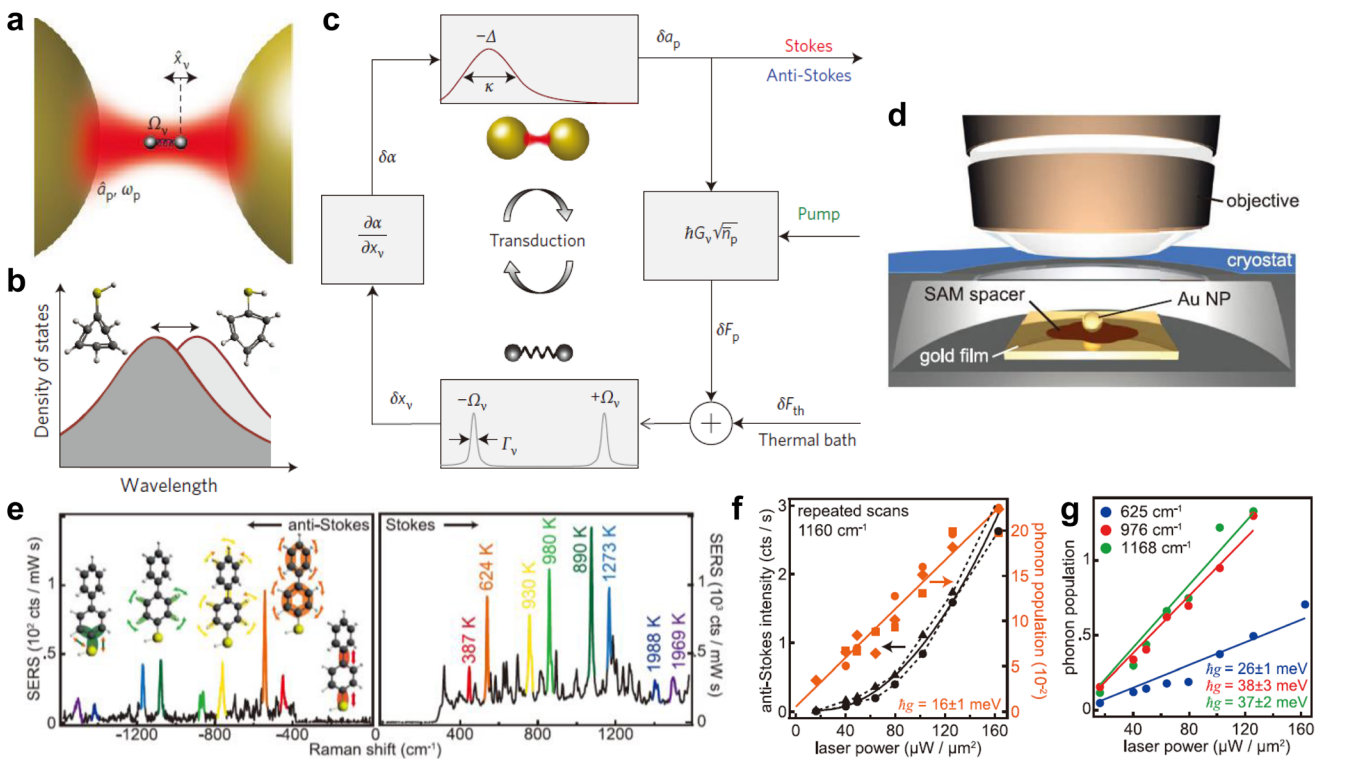

Fig. 4 Cavity optomechanical coupling between plasmon and molecular vibration. (a) Schematic diagram of a plasmonic hot spot hosting a molecule with a vibrational mode. (b) The molecule vibration leads to a change of molecule polarizability, which brings about the change of plasmonic resonance frequency. This is the origin of the parametric optomechanical coupling. (c) Schematic diagram of optomechanical feedback. Variables (fluctuations from average) are indicated along the arrows, and boxes represent transfer functions. δa_p is the plasmonic field. δF_p and δF_{th} are the plasmonic force and thermal force, respectively. δx_v is the molecule displacement. $\delta\alpha$ is the change of polarizability. Reprinted with permission from ref. 90. Copyright 2016, Nature. (d) Experimental setup of a nanoparticle-on-mirror geometry. (e) Raman spectra at a time when additional picocavity-induced lines are present. The same lines on the Stokes and anti-Stokes sides are identified by colours, with vibrational eigenmodes and effective temperatures shown. (f) The laser power dependence of anti-Stokes scattering intensity and average phonon population for different measurements on the same picocavity. (g) The average phonon population for different vibrational modes *versus* different powers in the same picocavity. Reprinted with permission from ref. 96. Copyright 2016, American Association for the Advancement of Science.

frequency of molecular vibration is ultrahigh, reaching the terahertz level,[117] which provides a novel design method for ultrahigh-frequency cavity optomechanical devices.

In recent years, a number of molecule cavity optomechanical experiments have been reported.[96–99] The volume of the cavity which confines light is decreasing and overcomes the diffraction limit. Felix Benz and his colleagues found that individual atomic features inside the gap of a plasmonic nanoassembly[115] can localize light to volumes well below 1 cubic nanometre ("picocavities"), enabling optical experiments on the atomic scale.[96] The experimental setup is shown in Fig. 4(d). Individual gold nanoparticles are spaced above a planar gold substrate by a nanometre-thick self-assembled monolayer (SAM) of biphenyl-4-thiol. All measurements are implemented at cryogenic temperatures using a modified dark-field microscope and laser pumping at 633 nm. According to low-temperature SERS, prominent anti-Stokes SERS lines which are blue-shifted from the laser (Fig. 4(e)) appear always and only when the additional fluctuating Stokes lines are present. The effective temperatures of eigenmodes are shown in Fig. 4(e). The effective temperatures are different for each scattering line and increase with increasing vibrational energy, which provides clear proof that the vibrational populations are nonthermal and that the pumping contribution to the phonon population cannot be ignored. A quadratic power dependence of the anti-Stokes signal and a linear power dependence for the anti-Stokes/Stokes ratio (phonon population) on different nanoparticles at different times are shown in Fig. 4(f), which provides evidence for the presence of vibrational pumping. The phonon population of different modes which linearly change with increasing laser power are shown in Fig. 4(g). However, the slope of these linear fits differed for different nanoparticles, which suggests that the slope is a measure of picocavity geometry and different optomechanical coupling strengths. In a word, the authors used laser irradiation to move atoms in the nanoparticle and produced a "picocavity" that was stable at cryogenic temperatures, which enables cavity optomechanical experiments on the atomic scale. Their work set the foundation for experiment on nonlinear quantum optics at the single-molecule nanoscale.

3. Principles of cavity-less exciton optomechanics

3.1. Excitons in semiconductors

In a semiconductor, when the electron is excited by the photon from the valence band to the conduction band, it induces a positively charged hole in the valence band.[46] The hole and electron form a neutral bound state *via* Coulomb interaction F_{Coulomb}, which is called an exciton.[82] This process is shown in Fig. 5(a). In ionic crystals, the electron and the hole are tightly bound to each other within the same or nearest-neighbor unit cells. These excitons are called Frenkel excitons. In most semiconductors, electrons and holes are weakly bound due to the electrostatic shielding of Coulomb interactions by electrons in the valence band. These excitons are known as Wannier excitons.[82] In this review, only Wannier excitons in semiconductor materials are concerned. A Wannier exciton system is similar to a hydrogen atom system composed of an electron and a proton. Hence, the properties of excitons can be calculated with the effective mass approximation.[82] Within this approximation, the energy of excitons E can be obtained:

$$E(\boldsymbol{K}) = E_g + \frac{\hbar^2 \boldsymbol{K}^2}{2M} - \frac{R^*}{n^2}, \tag{3}$$

where the exciton wave vector $\boldsymbol{K} = \boldsymbol{k}_e + \boldsymbol{k}_h$, exciton mass $M = m_e + m_h$, and $\boldsymbol{k}_e$, $\boldsymbol{k}_h$, m_e and m_h are the wave vector and effective

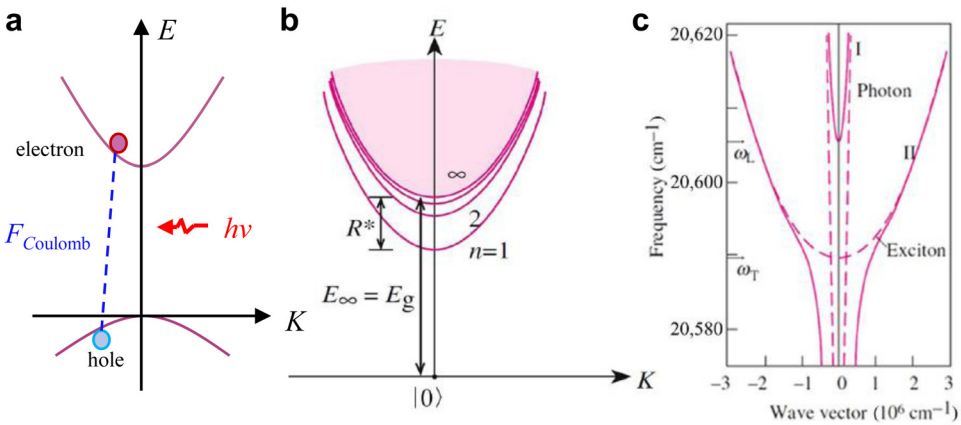

Fig. 5 Schematic diagram of Wannier excitons. (a) The generation of excitons in a semiconductor. $h\nu$ denotes incident photons and F_{Coulomb} is the Coulomb interaction. (b) Energy levels of a Wannier exciton from the bound states (n = 1, 2, and 3) to the continuum states. R^* is the Rydberg constant and E_g is the bandgap. (c) Dispersion curves of an exciton–polariton (solid curves labeled I and II). The curves labeled I and II are usually referred to as the "upper" and "lower" branches of the polariton. The dashed curves denote the dispersion curves of a "bare" exciton and a "bare" photon. Reprinted with permission from ref. 82. Copyright 2010, Springer.

mass of electrons and holes, respectively. R^* is the exciton binding energy and it can be calculated by

$$R^* = \frac{\mu e^4}{2\hbar^2 4\pi\varepsilon_0{}^2}, \quad (4)$$

where μ is the reduced mass of excitons. The energy spectrum of a Wannier exciton is shown in Fig. 5(b), a series of bound energy levels of excitons near the bottom of the conduction band are in the bandgap of the semiconductor, corresponding to the discrete peaks near the intrinsic absorption edge in the absorption spectrum.

The electric dipole moments of the excitons induce a polarization wave in the medium. The exciton polarized wave is formed with two branches, ω_T, and ω_L. The polarization wave coupling with the electromagnetic wave forms a "coupled state", which is called an exciton–polariton.[82,100,135] The dispersion curves of an exciton–polariton are shown in Fig. 5(c). As excitons travel in the medium, they radiate electromagnetic waves. Conversely, the electromagnetic wave can excite excitons in the semiconductor. In this picture, energy is converted between excitons and photons.

3.2. Exciton-mediated optomechanical forces

The existence of excitons gives rise to three kinds of optomechanical force in the exciton optomechanical system.[101] First, the opposite charges of electrons and holes result a large electric field, inducing piezoelectric shear stress. Second, the electron transition from the valence band to the conduction band increases the lattice constant, yielding a hydrostatic stress, which can be quantified by deformation-potential E_{dp}:[102]

$$E_{dp} = -B\mathrm{d}E_g/\mathrm{d}p \quad (5)$$

,where B is the bulk modulus, p is the pressure, and E_g is the band gap. Third, the nonradiative relaxation of excitons gives rise to temperature gradients in the optomechanical system, known as photothermal strain. The exciton optomechanical system is operated at low temperatures because exciton linewidth broadens with increasing temperature. The coefficient of thermal expansion for the III–V semiconductors in low temperatures is minimal, which is opposite to the low-dimensional semiconductor systems. Hence, the photothermal effect in exciton optomechanical systems based on semiconductor quantum wells in low temperatures can be neglected,[101] while for the low-dimensional exciton optomechanical system, the photothermal effect could not be neglected.[45]

Andreas Barg *et al.* investigated carrier-mediated optomechanical forces in semiconductor nanomembranes with coupled quantum wells.[101] The free-free nanomembranes with embedded CQWs are shown in Fig. 6(a and b). They used long-lived indirect exciton states in the CQWs as frequency-matched mediators of optomechanical forces. The lifetime of indirect exciton states is tunable over two orders of magnitudes *via* the bias voltage V_b. Based on the properties of indirect excitons, they simulated modulated acceleration $a_{eh}(\Omega_m)$ for piezoelectric and deformation-potential coupling using finite-element methods. As shown in Fig. 6(c and d), they obtain the calculated amplitude and phase of $a_{eh}(\Omega_m)$ as a function of the

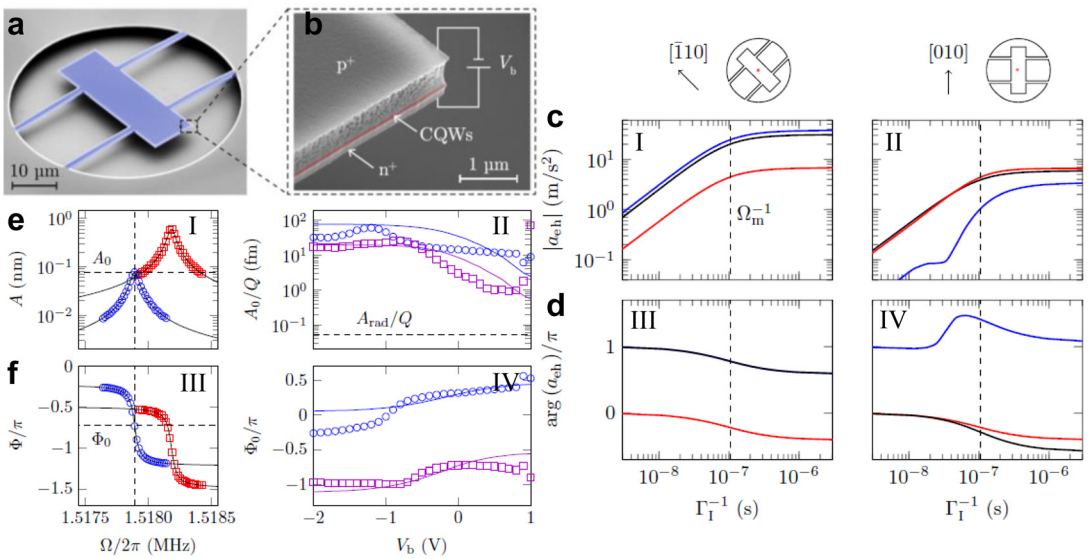

Fig. 6 Exciton-mediated optomechanical forces. (a) False-color SEM image of free–free nanomembranes with embedded CQWs. (b) Close-up of the vertical position of the CQWs. (c, d) Simulation of the amplitude (I, II) and phase (III, IV) of the acceleration $a_{eh}(\Omega_m)$ mediated by piezoelectricity and the deformation potential in crystallographic directions [$\bar{1}$10] and [010] for different bias voltages, here 0 V (blue curves) and −1 V (red curves). (e, f) The rms amplitude A (I) and phase Φ (III) of the symmetric bending mode as a function of the modulation frequency. Normalized peak rms amplitude A_0/Q (II) and phase Φ_0 (IV) *versus* bias voltage V_b as measured for two different membrane orientations, [$\bar{1}$10] (blue circles) and [010] (purple squares). The solid lines are fitting lines. Reprinted with permission from ref. 101. Copyright 2011, American Physical Society.

exciton lifetime in two different crystallographic orientations, [$\bar{1}$10] and [010] (Miller indices). According to the related results, if the long edges of the rectangular membrane are parallel to [$\bar{1}$10], the piezoelectric force dominates. If the long edges of the rectangular membrane are parallel to [010], the membrane is driven by the deformation-potential. As shown in Fig. 6(e and f), they concluded that the exciton-mediated forces studied here are significantly stronger than the radiation pressure and the optomechanical forces form a deformation-potential, and the piezoelectric effect can be tuned by the bias voltage V_b. Their work paves a way for us to understand the source of optomechanical forces in the cavity-less exciton optomechanical systems.

3.3. Strain tuning exciton resonance

In cavity-less exciton optomechanics, the optomechanical feedback mainly comes from the exciton resonance detuned by strain *via* opto-piezoelectric backaction because the linewidth of the exciton resonance is orders of magnitude larger than the mechanical resonance frequency, which makes it difficult to achieve efficient optomechanical self-feedback through the phonon–exciton parametric coupling.[42] Strain engineering[103–105] is an efficient way to tune the electronic properties of the materials and explore novel quantum states, which leads to an emerging research field known as "straintronics".[106] The two-dimensional materials are suitable candidates for exciton optomechanics because exciton resonance in two-dimensional materials is stronger than that of bulk materials as a result of spatial constraints and poor dielectric screening in the two-dimensional materials.[107,108] The strain effect on the electronic and vibrational properties of two-dimensional materials has been extensively investigated. Transition metal dichalcogenides (TMDs) with lower symmetry and strong excitonic effects offer an excellent opportunity for exciton resonance tuning *via* strain engineering.[109] The strain tuning exciton resonance in TMDs has been investigated from theoretical prediction and experiments. Keliang He *et al.* first demonstrated the continuous tuning of the exciton resonance of atomically thin MoS_2 on flexible substrates by applying a uniaxial tensile strain in 2013.[110] In the following, we present an introduction to their work on strain tuning exciton resonance.

The experimental setup is shown in Fig. 7(a). A flexible and transparent PMMA substrate was used to apply controllable and reproducible strains on the MoS_2 samples. A layered MoS_2 sample was deposited on the PMMA by mechanical exfoliation of bulk MoS_2 crystals. The layer numbers of the MoS_2 sample

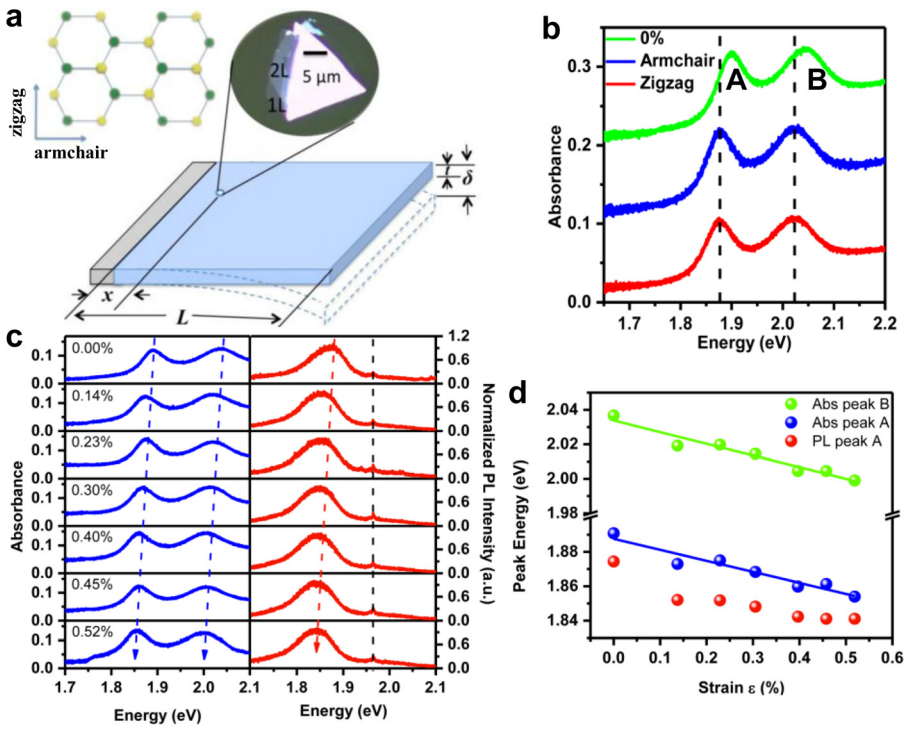

Fig. 7 Exciton resonance tuning *via* strain in atomically thin MoS_2. (a) Schematic diagram of a cantilever used in the experiment. The length L and thickness t of the square-shaped PMMA substrate are 9.5 cm and 0.245 cm, respectively. Mechanically exfoliated MoS_2 samples were deposited near a corner of the substrate. Strain was applied on the samples by clamping one edge (gray) and bending the opposite edge of the substrate. The left inset is the atomic structure of monolayer MoS_2. The right inset is the optical image of one sample with both a monolayer (1L) and bilayer (2L). (b) Absorption spectrum of a monolayer MoS_2 sample for strain (0.4%) applied along the armchair and zigzag direction. (c) Absorption and PL spectrum of a monolayer MoS_2 sample under tensile strains up to 0.52% along the zigzag direction. The black dashed line at 1.96 eV is the PMMA Raman line at 2954 cm^{-1}, which is independent of strain. (d) Strain dependence of the absorption peak A, B and PL peak A. Reprinted with permission from ref. 110. Copyright 2013, American Chemical Society.

can be identified by their optical contrast. In the cantilever setup, strain of a certain direction can be applied on the MoS_2 sample by bending the flexible substrate in zigzag or armchair directions because of the van der Waals coupling at the sample–substrate interface. The absorption spectrum of atomically thin MoS_2 samples was measured to determine the exciton resonance energy. The photoluminescence spectroscopy (PL) was measured to determine the indirect gap transitions due to weak absorption. The absorption spectrum of the MoS_2 monolayer under 0.4% strain along the armchair and zigzag directions is shown in Fig. 7(b). Compared with the absorption spectrum under no strain, both the A and B exciton features exhibit a redshift and no difference is observed for the two distinct strain directions, which indicated that the exciton resonance shift is independent of the strain direction.

The absorption spectrum and PL spectrum of monolayer MoS_2 under strain along the zigzag direction are shown in Fig. 7(c). The PL spectra are normalized to the A exciton peak. Both the A and B exciton absorption peaks redshift with increasing strain. As shown in Fig. 7(d), a linear dependence is observed for the relatively small strains investigated here. The A exciton PL peak shows a similar strain dependence and a redshift rate compared with the A exciton absorption peak, which demonstrates that the Stokes shift in this sample is largely strain independent. However, the Stokes shift of the A exciton PL is strain dependent for the bilayer MoS_2 sample, likely due to strain-induced defects. Their work demonstrates that strain can tune exciton resonance energy in two-dimensional materials, which opens a new opportunity for applications of 2D crystals in exciton optomechanics and provides a toolbox to understand feedback in exciton optomechanical systems.

4. Progress of cavity-less exciton optomechanical coupling

4.1. Resolved sideband Raman cooling of optical phonons in semiconductors

Brillouin cooling and amplification of acoustic modes have been demonstrated in whispering-gallery optomechanical systems.[6] In 2016, Zhang Jun *et al.* reported laser cooling longitudinal optical phonons (LOPs) in ZnTe nanobelts with the assistance of exciton resonance.[44] The vibrational normal mode of an LOP in shown in Fig. 8(a). The vibration of long-wavelength LOPs leads to the separation of oppositely charged atoms and generates a macroscopic electric field inside the crystals. The electric field of the excitons interacts with the macroscopic electric field *via* Fröhlich forces. The Fröhlich forces that act on the optical phonons will exert work on the phonon oscillation. The vibration of phonons can be enhanced (heating) or attenuated (cooling) depending on the positive or negative work acting on the phonons. The coupling between excitons and optical phonons forms a novel quasiparticle, the so-called polaron (Fig. 8(b)). In the cavity optomechanical systems, the "cavity" plays two roles: on one hand, the resonant cavity enhances the number of photons in the cavity; on the other hand, the change of the length of the cavity realizes the coupling between photons and mechanical oscillators. In cavity-less exciton optomechanical systems, the excitons coupled with photons enhanced the number of photons and the strain tunes exciton resonance, which induces exciton-optomechanical coupling. Hence, excitons act as an "optical cavity in a cavity optomechanical system", which enhances the coupling between the excitation laser and optical phonons.

The basic principle and experimental set-up of resolved sideband cooling and heating are shown in Fig. 8(c–f). The detuned frequency between the laser and exciton is defined such that $\Delta = \omega_{\mathrm{laser}} - \omega_{\mathrm{exciton}}$, where ω_{laser} is the frequency of the laser and $\omega_{\mathrm{exciton}}$ is the frequency of exciton resonance. The cooling experimental setup is shown in Fig. 8(c). The red-detuned laser beam ($\Delta = -\Omega_{\mathrm{LO}}$) was used to pump the system, where Ω_{LO} is the frequency of the LOP. The anti-Stokes scattering process is enhanced by the exciton resonance, and thus the thermal vibration quanta of the LOP from the ZnTe can be cooled down. The blue-detuned laser beam ($\Delta = \Omega_{\mathrm{LO}}$) was used to probe the cooling behaviour of the LOP by monitoring its Stokes components. As shown in Fig. 8(d), a red-detuned driving laser will add extra damping, Γ_{net}, into the intrinsic LOP damping, Γ_0, and decrease its occupation number $\bar{n}_{\mathrm{LO}}$. The corresponding experimental results are shown as red curves in Fig. 8(h), in which the Stokes scattering is suppressed and anti-Stokes scattering is enhanced. The cooling results are shown in Fig. 8(g). With increasing the cooling pumping power from 0 to 1.1 mW, the occupation number $\bar{n}_{\mathrm{LO}}$ decreases from 0.36 to 0.19 with an increase corresponding to the ground-state occupation possibility from ~73.5 to 84.0% and an effective temperature decrease from 225 to 165 K. The heating experimental set-up is shown in Fig. 8(e). The blue-detuned laser beam ($\Delta = \Omega_{\mathrm{LO}}$) was used to pump the exciton optomechanical system. The Stokes scattering process is enhanced and anti-Stokes scattering process is suppressed, as shown in the blue curves in Fig. 8(h). Hence, the thermal vibration quanta of the LOP can be amplified (Fig. 8(f)) and the linewidth of the LOP decreases. The heating results are shown in Fig. 8(i). The occupation number and effective temperature of the LOP changed linearly with the heating pumping power, which suggests LOP lasing was not observed in the experiment. LOP lasing in the order of terahertz frequency is important for terahertz applications. One possible solution is increasing the power of the pump laser, because the pump laser power in the experiment may not reach the threshold of LOP lasing. Another possible solution is fabricating a cavity composed of this ZnTe nanostructure or putting ZnTe gain materials into another optical cavity. This work realized strong coupling between photons and LOPs by exploiting the strong exciton resonance in the ZnTe semiconductor, which leads to Raman cooling of LOPs. This result provides a possible experimental method to achieve a net Raman cooling of solids.

However, due to the very large exciton linewidth in this experiment, the resolved sideband Raman cooling is only limited to high-frequency optical phonons and is not feasible

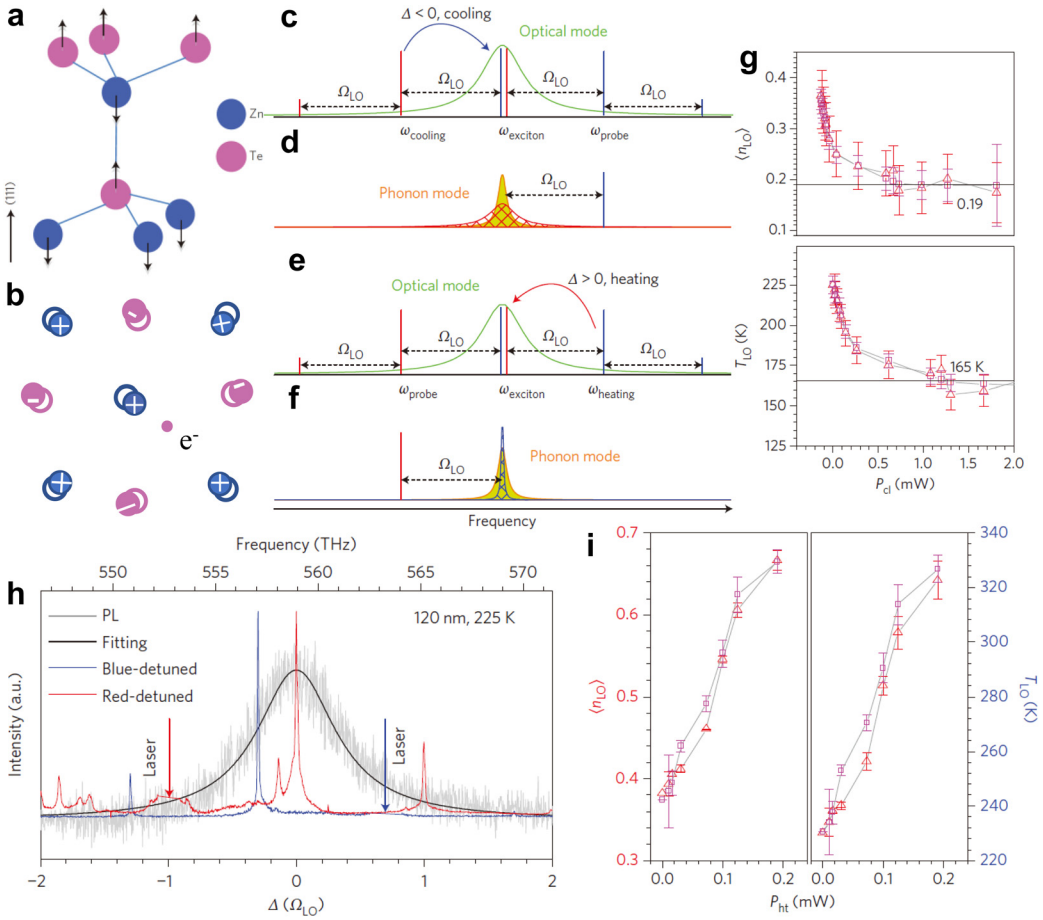

Fig. 8 Resolved-sideband Raman cooling LOP with exciton resonance. (a) Schematic diagram of the vibrational normal mode of the LOP in ZnTe. (b) Polaron: a new quasiparticle of the exciton–LOP coupling. (c) Principle and detection method of red-detuned laser cooling in the semiconductor. (d) With increasing cooling laser power, the LOP's phonon occupation number decreases and its damping rate increases. (e, f) Principle and detection method of blue-detuned laser amplification in the semiconductor. (g) Occupation number and temperature of the LOP *versus* cooling laser power. (h) The measured experimental spectra of exciton transition. The red curves are the Stokes spectra of an LOP with red-detuned laser. The blue curves are the anti-Stokes spectra of an LOP with blue-detuned laser. (i) Occupation number and temperature of an LOP *versus* heating laser power. Reprinted with permission from ref. 44. Copyright 2016, Nature.

for low-frequency acoustic phonons because in the sideband-resolved regime, the optical decay should be smaller than the mechanical frequency *i.e.*, $\kappa_0 < \Omega_m$. Hence, semiconductor materials with narrower exciton linewidths are feasible to achieve resolved sideband cooling acoustic phonons. This work was implemented based on ZnTe nanobelts. However, for practical tasks, it is desirable to cool larger volumes, and that is hard to achieve because of inherently weak Raman processes and inevitable heating.[132] Recently, Jia-Min Lai *et al.* reported laser cooling of optical phonons in a van der Waals semiconductor cavity-less exciton optomechanical system,[133] which is progress in achieving laser cooling in larger volumes than reported previously.

4.2. On-chip optomechanics using excitonic transitions in semiconductor heterostructures

In the section 4.1, we introduced the resolved sideband cooling LOPs in cavity-less exciton optomechanical systems, while in this part we will introduce optomechanical amplification/damping *via* the strain-induced modulation of exciton number in an exciton optomechanical system which was first reported by Hajime Okamoto *et al.* in 2015.[42] In this system, when the pump photon energy is blue (red) detuned, it leads to damping (amplification), which is opposed to resolved sideband cooling/heating. The GaAs/AlGaAs cantilever exciton optomechanical device is shown in Fig. 9(a). According to the photoluminescence excitation (PLE) spectrum in Fig. 9(e), the exciton resonance energy is around 1.5152 eV. The intensity of the incident Ti:Sa laser was sinusoidally modulated, while the frequency was swept around the fundamental mechanical mode. The frequency of mechanical motion was measured in a vacuum by Doppler interferometry with a He:Ne laser (633 nm). When the energy of the pump photon is set to the excitonic resonance energy (1.5252 eV), the frequency response of mechanical motion shows Lorentzian resonance (Fig. 9(b)). As shown in Fig. 9(d), the photon-energy dependence of the

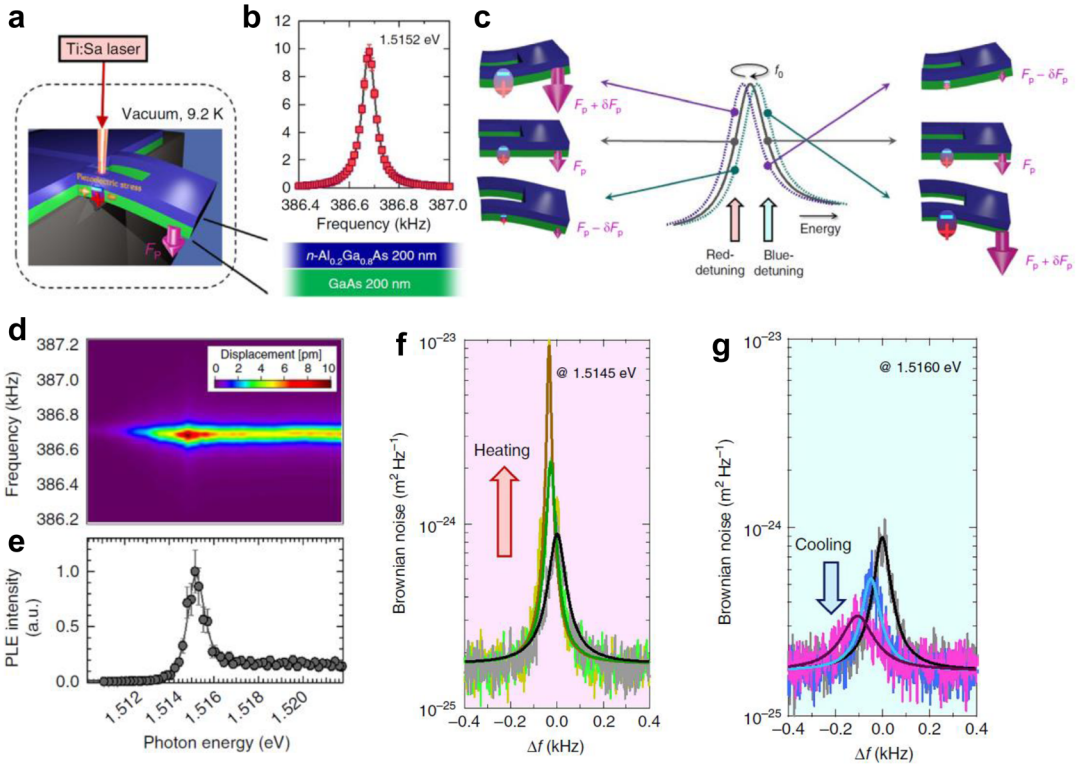

Fig. 9 Exciton optomechanics in semiconductor heterostructures. (a) Schematic diagram of the opto-piezoelectric effect mediated by excitons. (b) Frequency response of the cantilever when the photons' energy tuned to the exciton resonance (E_e = 1.5152 eV). (c) Schematic diagram of the strain-modulated exciton resonance and the strain-dependent opto-piezoelectric backaction for red and blue detuning. (d) Photon-energy dependence of the frequency response under modulated illumination. (e) Photoluminescence excitation (PLE) spectrum, and a sharp exciton resonance at 1.5152 eV. Noise power spectrum for photon energy (1.5145 eV) red (f) and blue (g) detuned from exciton resonance for different laser powers. Reprinted with permission from ref. 42. Copyright 2015, Nature.

frequency response reveals that the vibration amplitude is maximized at the exciton resonance energy.

The cavity-less exciton optomechanical coupling driven by the opto-piezoelectric effects follows the following mechanism: electrons and holes excited by photo in the GaAs layer are separated by the built-in electric field along the thickness direction, which generates a dipole moment. It leads to a piezoelectric bending moment as if the cantilever is driven by a vertical backaction force F_p (Fig. 9(a)). The vibration amplitude of the cantilever is sensitive to photon energy (Fig. 9(d)) because F_p is proportional to the number of excitons contributing to the opto-piezoelectric backaction. This provides a novel mechanical method of probing the optical transitions.

As shown in Fig. 9(c), the exciton resonance in this optomechanical system can be modulated by strain *via* the deformation potential.[111] The exciton resonance red shifts (blue shifts) when the cantilever bends upwards (downwards). Hence, when the incident photon energy red-detunes from exciton resonance, the upwards bending increases the dipole moment with an increase of absorption, leading to an increase in the backaction force ($F_p + \delta F_p$), while downwards bending decreases the dipole moment with a decrease of absorption, leading to a decrease in the backaction force ($F_p - \delta F_p$). In the red-detuned regime, the sign of the force gradient $\partial F_p/\partial z$ is negative, where z is the displacement of the cantilever. The negative $\partial F_p/\partial z$ and the time delay $\tau \sim {\omega_0}^{-1}$ coming from the spatial separation of electrons and holes in the cantilever lead to an amplification of the mechanical vibration, where ω_0 is the frequency of mechanical vibration. The Brownian displacement noise power spectrum of the cantilever when the photon energy is red detuned (1.5145 eV) is shown in Fig. 9(f). With the increasing laser power, the vibration amplitude increases and the linewidth of the resonance becomes narrow. In the blue-detuned regime, the positive $\partial F_p/\partial z$ and time delay lead to damping. As shown in Fig. 9(g), with the increasing laser power, the vibration amplitude decreases and the linewidth of the resonance becomes wide, indicating cooling of the mechanical mode. The process above is opposite to sideband amplification/damping. In this cavity-less exciton optomechanical system, the polarity of the feedback is determined by the sign of the slope in the PLE spectrum and the sign of the piezoelectric coefficient. The backforce in this exciton optomechanical system is not caused by phonon–exciton parametric coupling, but by carries-induced piezoelectric force. Besides, the retarded backaction contributed to the cooling as well as amplification of the mechanical mode without any optical cav-

ities. Besides, the gain of the opto-piezoelectric self-feedback depends on the mechanical quality factor Q_m and it is important to design higher Q_m resonators in order to improve the feedback efficiency. This work is a significant progress in cavity-less exciton optomechanics. It developed a more scalable 'cavity-less' optomechanical scheme that also allows free-space optical access and achieved highly tunable vibration control of nanomechanical resonators.

4.3. Electrically driven tunable exciton-optomechanical coupling

Two-dimensional semiconductor materials and graphene have attracted tremendous interest and have been extensively studied in nanoelectromechanical systems because of their mechanical flexibility,[63,112] gate-tunability[57,113] and strong mechanical nonlinearity.[114] However, there is little literature about exciton optomechanical coupling in two-dimensional semiconductor materials. The strong exciton resonance in monolayer TMD semiconductors could interact with light strongly, which is a suitable platform to study cavity-less exciton optomechanical coupling. Besides, semiconductor materials with a tunable direct bandgap and high carrier mobility, such as monolayer transition metal dichalcogenides and black phosphorus, are suitable candidates for tunable exciton optomechanical coupling. Hongchao Xie and his colleagues demonstrated gate-tunable exciton optomechanical coupling in suspended monolayer $MoSe_2$ (Fig. 10(a)).[45] The circular trenches were obtained on a SiO_2/Si substrate using photolithography and reactive ion etching. The gold electrodes were deposited next to the circular trenches and the suspended $MoSe_2$ monolayers were mechanically exfoliated from bulk crystals and transferred onto the targeted trench.

In this work, reflection contrast spectra were measured to detect the exciton resonance. The reflection contrast spectra were obtained by normalizing the reflected light intensity from the suspended $MoSe_2$ region to that from a bare circular

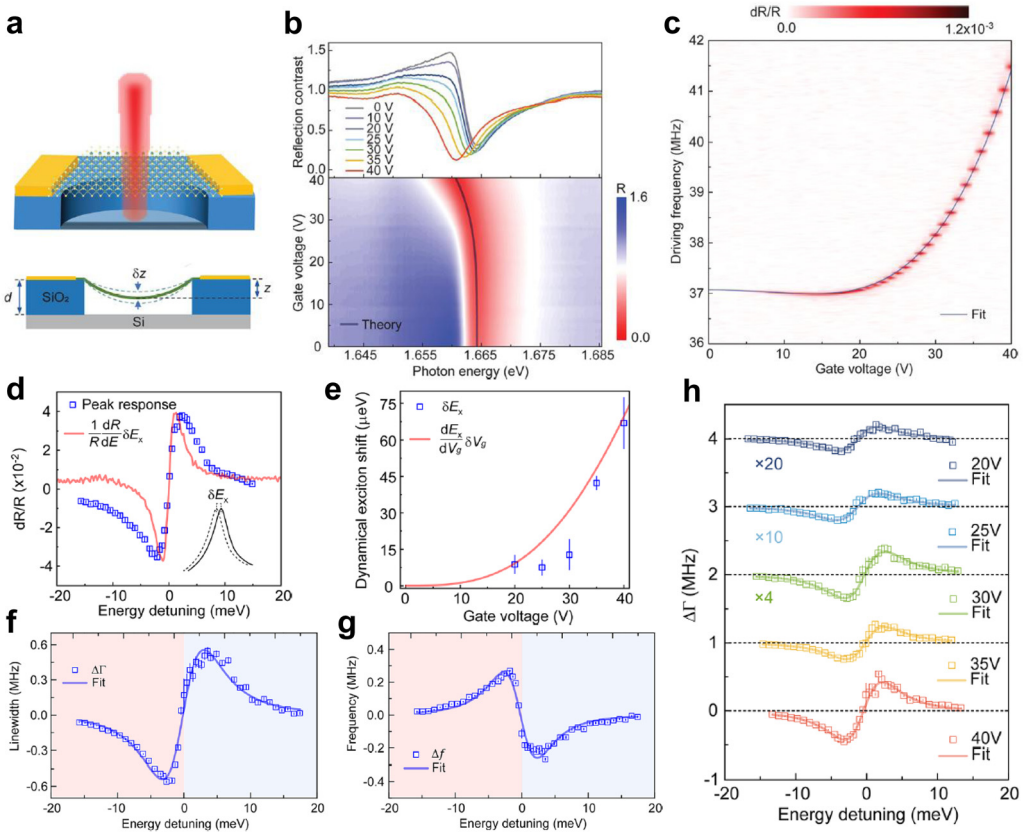

Fig. 10 Gate tunable exciton-optomechanical coupling. (a) Schematic diagram of monolayer MoS_2 optomechanical devices. (b) Reflection contrast spectrum of suspended monolayer $MoSe_2$ at different gate voltages. The solid line in the bottom panel is the expected dependence of the exciton resonance energy. (c) Gate voltage dependence of the mechanical resonance frequency. (d) The peak response of the fractional change in reflection contrast as a function of the probe photon energy detuning from the exciton resonance. The red curve is the energy derivative of the normalized reflection contrast spectrum with V_g = 40 V multiplied by the dynamic exciton displacement with a peak-to-peak amplitude of $\delta E_X \approx 67$ μeV. The inset is a schematic diagram of the dynamic shift in exciton resonance. (e) The gate voltage dependence of δE_X extracted from a similar measurement as in (d) at different gate voltages. The red curve is the expected dependence $(dE_X/dV_g)\delta V_g$ extracted from the solid line in (b) at δV_g = 200 mV. The mechanical linewidth (f) and resonance frequency (g) as a function of incident photon energy detuning from exciton resonance. The blue- and red-shaded regions correspond to blue and red energy detuning, respectively. (h) The backaction-induced change in mechanical line width as a function of the energy detuning at selected gate voltages. Reprinted with permission from ref. 45. Copyright 2021, American Chemical Society.

trench without $MoSe_2$. The reflection contrast spectra of the sample at varying gate voltages (0–40 V) are shown in Fig. 10(b). The exciton resonance red shifts with increasing gate voltage because of the in-plane strain at the sample. The vibration of the membrane was measured by a network analyser. The gate voltage dependence of the fundamental mechanical mode in a contour plot was shown in Fig. 10(c). The mechanical resonance frequency slightly decreases at first and increases then with increasing gate voltages, which can be explained by gate modulation of the effective spring constant of the device (solid fit line in Fig. 10(c)).

The exciton optomechanical coupling was investigated by detecting the spectral dependence of the mechanical response. They varied the photon energy near the exciton resonance energy and obtained the fractional change in reflectivity dR/R (peak to peak value) at V_g = 40 V. The peak response *versus* photon energy detuning ($\Delta E \equiv E - E_x$) from exciton resonance energy is shown in Fig. 10(d), where E is the incident photon energy, and E_x is the resonance energy. They studied energy detuning ΔE instead of the absolute photon energy E in order to rule out the red shifts of the exciton resonance caused by laser heating. The spectral response can be understood as that a dynamical shift in the exciton resonance (δE_x) was induced by strain in the monolayer (as shown in the inset in Fig. 10(d)). This provides a relationship between the fractional change in reflectivity and mechanical resonance:

$$dR/R = \frac{1}{R}(dE/dR)\delta E_x. \quad (6)$$

The quantity $(dE/dR)/R$ can be calculated from the measured reflection contrast spectrum in Fig. 10(b). To match the calculated red curve with data points (dR/R), δE_x is treated as a variable and $\delta E_x \approx 67$ μeV approximately at V_g = 40 V. The same analysis is performed at each voltage V_g as shown in Fig. 10(e). The result confirms the picture of dynamical exciton spectral shift and shows a monotonic increase in the exciton-mechanical coupling strength with V_g.

The dynamic feedback was studied by optical detection in fundamental mechanical mode at varying incident photon energies (V_g = 40 V). The incident power is increased from 1 μW to 10 μW in order to amplify the dynamical backaction. The shift in the mechanical resonance (frequency and linewidth) is asymmetric with photon energy detuning (Fig. 10(f and g)). For large detuning from the exciton resonance, the fundamental mechanical mode is largely unperturbed by the incident light. However, the mechanical resonance red shifts and the linewidth broadens with asymmetric detuning dependences. The phenomena can be understood in a model based on photothermal backaction and gate-induced mirror symmetry breaking in the mechanical device. The $MoSe_2$ membrane is pulled down by the electrostatic force from the back gate, which breaks the out-of-plane mirror symmetry of the device. The strain induced by mechanical vibration leads to an exciton resonance shift. The dynamical shift in turn periodically modulates the photothermal force F_{ph} produced by laser illumination near the exciton resonance. The magnitude and phase of F_{ph} depend on the detuning ΔE from the exciton resonance. The detuning dependences of the antisymmetric contribution of the mechanical line width at varying V_g are shown in Fig. 9(h). The amplitude of the antisymmetric contribution (half of the peak-to peak height in the detuning dependences) increases quickly with V_g, which also demonstrates gate-tunable exciton-optomechanical coupling strength.

In this work, the authors demonstrated dynamical light control of the mechanical motion of suspended monolayer $MoSe_2$ through the strong excitonic resonance of the TMDs. The gate-tunable exciton optomechanical coupling can be realized by detuning the exciton resonance energy δE_x based on photothermal backaction. Keliang He *et al.* demonstrated that exciton resonance detuning in monolayer and bilayer TMD (MoS_2) under strain is different.[110] Hence, the layer number of the two-dimensional materials may have an effect on the exciton optomechanical coupling, which requires our further research.

4.4. Cavity-less exciton-optomechanical coupling for detection of coherent phonons with high sensitivity

As mentioned in section 2.3, the photon–phonon interaction can be enormously enhanced by exciton-polaritons in the microcavity composed of a semiconductor superlattice. At the same time, the semiconductor superlattice is also a platform for the realization of cavity-less exciton optomechanical coupling. M. Kobecki and his colleagues discovered a giant photoelasticity of exciton-polaritons in a short-period superlattice and exploited it to detect propagating acoustic phonons.[118] They demonstrated that high-frequency coherent acoustic phonons could be detected with extremely high sensitivity in the spectral vicinity of the polariton resonance.

The experimental setup is shown in Fig. 11(a). The superlattice grown on a GaAs substrate consists of 30 periods of GaAs and AlAs layers with thicknesses of 12 nm and 14.2 nm, respectively. The resonance energy ($\hbar\omega_0$) of the polariton is 1.55 eV (Fig. 11(b)). The aluminium films deposited on the GaAs substrate backside. When the film is excited using the pump laser pulses, a wave packet of coherent acoustic phonons is generated and propagates through the GaAs substrate with the velocity of longitudinal sound ν = 4800 m s^{-1}. The coherent phonons are detected in the superlattice by measuring the reflectivity changes $\Delta R(t)$ of an optical probe pulse. The detected transient signal around the polariton resonance is shown in Fig. 11(c). When -150 ps $\leq t \leq$ 150 ps, the wave pocket of the coherent phonons propagates through the superlattice toward the free surface. To study the effect of the superlattice polariton resonance on the TDBS signal, the authors measured the TDBS signal $\Delta R(t)$ for different central photon energies $\hbar\omega$. The value of $\hbar\omega$ is varied between 1.544 and 1.556 eV, which is in the vicinity of the polariton resonance. It is seen that the amplitude of the oscillations strongly depends on the probe pulse photon energy (Fig. 11(d)). As shown in Fig. 11(e), the dependences are symmetric for amplitude (A_B) and decay rates (τ_B^{-1}) and antisymmetric for frequency (f_B) and phase (p_B) relative to $\hbar\omega_0$, which means that

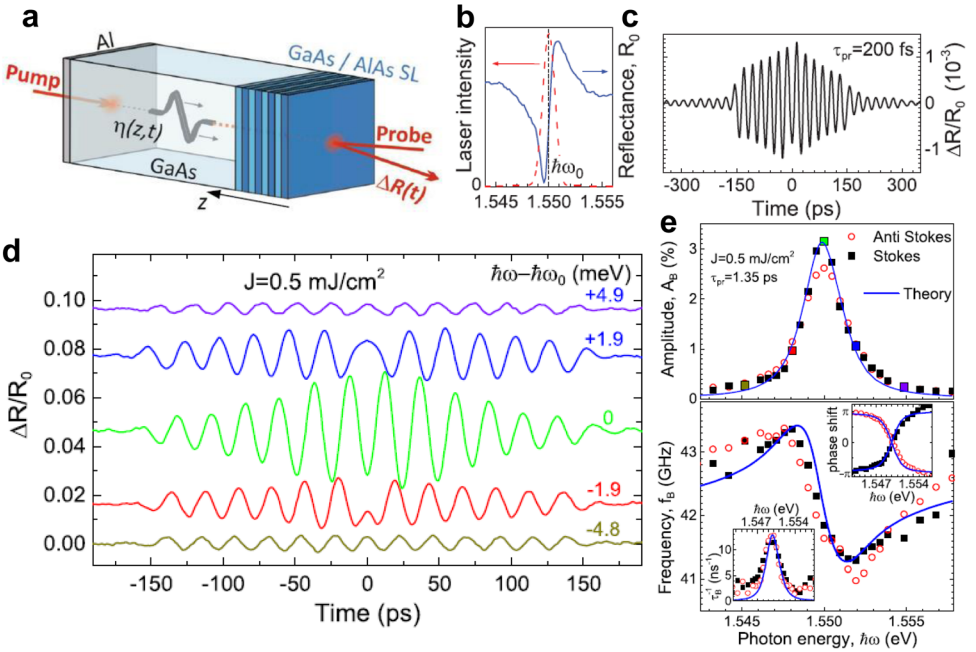

Fig. 11 Cavity-less exciton optomechanical system for the detection of coherent phonons in a semiconductor superlattice. (a) Schematic diagram of the experimental setup. (b) Reflectivity spectrum in the vicinity of the polariton resonance (blue curve) and the spectrum of the spectrally narrow probe pulse centred at the polariton resonance (red dashed curve). (c) Time domain Brillouin scattering (TDBS) signal measured with probe pulses of 200 fs duration. "t = 0" corresponds to the arrival of the phonon wave packet centre at z = 0. (d) TDBS signals measured by the spectrally narrowed probe pulses for several $\hbar\omega$. (e) Dependences of the specific properties of the TDBS signals on the probe photon energy: amplitude (A_B), frequency (f_B), decay rate τ_B^{-1}, and phase shift.

the TDBS signals are governed by the polariton resonance when probing with $\hbar\omega$ close to $\hbar\omega_0$. The relative changes $\Delta R/R_0$ are $\sim 10^{-2}$ for the used pump fluence $J \sim 0.1$ mJ m^{-2}, which is three orders of magnitude higher than that previously reported.[119,120] This result means that their experiments reveal a giant photoelasticity of polaritons and extremely high sensitivity to detecting coherent phonons.

In a word, their work demonstrated that 42 GHz coherent phonons can be detected with extremely high sensitivity in the cavity-less exciton optomechanical system composed of the semiconductor superlattice. Moreover, coherent acoustic phonons are suggested to become a logistic element in quantum computer networks[121–123] and have been demonstrated to be promising in quantum technologies and nanophononics.[124–126] Hence, their work provides a method to generate and detect high-frequency acoustic phonons in optomechanical systems without an optical resonant cavity, and a new toolbox for quantum technologies based on phonons.

5. Conclusions and perspectives

In cavity optomechanical system coupling by radiation pressure or photothermal forces, the mechanical displacement of the end mirror of an optical cavity dynamically changes the cavity resonance frequency, which in turn periodically modulates the intracavity optical field and the radiation pressure or photothermal forces on the mirror with a time delay given by the photon storage time. The delayed effect creates a dynamical backaction on the mirror's mechanical displacement and produces the well-known optical spring effect and optical damping. In cavity optomechanical system coupling by a photoelastic effect, the dynamic backaction comes from the mechanical amplification or damping caused by the electrostrictive interference pattern. In the cavity-less exciton optomechanical system, the optical resonance cavity is replaced by exciton resonance. The mechanical vibration of the sample causes a strain in the sample, which in turn produces a shift in the exciton resonance due to the strain dependence of the exciton resonance energy. The time delay coming from the spatial confinement of free e–h pairs to form their bound state causes cooling or amplification mechanical vibration without any optical cavities.

Cavity-less exciton optomechanics is still a new field of optomechanical research and it has not attracted as much attention as cavity optomechanics. The on-chip cavity-less exciton optomechanical system is an optomechanical system with the advantages of easy integration, strong optomechanical coupling, and highly tunable mechanical vibrations compared with cavity optomechanical systems. The simultaneously strong optical and mechanical nonlinearity in the TMDs cavity-less exciton optomechanical devices would be a new platform for fundamental studies and applications, such as chaos, optomechanical solitons and so on. Besides, the band

engineering may provide a method to alert the optomechanical coupling in exciton optomechanical devices composed of 2D semiconductor materials. The ultrahigh-frequency (~terahertz) exciton optomechanical systems could reach a quantum ground state at high temperature, which will pave the way to a robust quantum control of phonons and provide the implementation of efficient ultrafast quantum information protocols. However, for cavity optomechanics, reaching a terahertz frequency is very difficult. Hence, cavity-less exciton optomechanical systems are a very promising platform for realizing sensing, signal processing and other functions in integrated optomechanical devices. Cavity-less exciton optomechanics will be a promising research field in the future.

Conflicts of interest

There are no conflicts to declare.

Acknowledgements

J. Z. acknowledges the funding support from the National Key Research and Development Program of China (2017YFA0303401), CAS Interdisciplinary Innovation Team, National Natural Science Foundation of China (12074371), Strategic Priority Research Program of Chinese Academy of Sciences (XDB28000000).

References

1 M. Aspelmeyer, T. J. Kippenberg and F. Marquardt, Cavity optomechanics, *Rev. Mod. Phys.*, 2014, **86**(4), 1391–1452.
2 V. B. Braginsky and A. B. Manukin, Pondermomtive effects of electromagentic radiation, *Sov. Phys. JETP*, 1967, **25**, 653–655.
3 A. Dorsel, J. D. McCullen, P. Meystre, E. Vignes and H. Walther, Optical bistability and mirror confinement induced by radiation pressure, *Phys. Rev. Lett.*, 1983, **51**(17), 1550–1553.
4 J. Mertz, O. Marti and J. Mlynek, Regulation of a microcantilever response by force feedback, *Appl. Phys. Lett.*, 1993, **62**, 2344.
5 C. H. Metzger and K. Karrai, Cavity cooling of a microlever, *Nature*, 2004, **432**, 1002–1005.
6 G. Bahl, M. Tomes, F. Marquardt and T. Carmon, Observation of spontaneous Brillouin cooling, *Nat. Phys.*, 2012, **8**(3), 203–207.
7 L. Mercadé, K. Pelka, R. Burgwal, A. Xuereb, A. Martínez and E. Verhagen, Floquet phonon lasing in multimode optomechanical systems, *Phys. Rev. Lett.*, 2021, **127**(7), 073601.
8 R. M. Pettit, W. Ge, P. Kumar, D. R. Luntz-Martin, J. T. Schultz, L. P. Neukirch, M. Bhattacharya and A. N. Vamivakas, An optical tweezer phonon laser, *Nat. Photonics*, 2019, **13**(6), 402–405.
9 K. Vahala, M. Herrmann, S. Knünz, V. Batteiger, G. Saathoff, T. W. Hänsch and T. Udem, A phonon laser, *Nat. Phys.*, 2009, **5**(9), 682–686.
10 I. S. Grudinin, H. Lee, O. Painter and K. J. Vahala, Phonon laser action in a tunable two-level system, *Phys. Rev. Lett.*, 2010, **104**(8), 083901.
11 D. L. Chafatinos, A. S. Kuznetsov, S. Anguiano, A. E. Bruchhausen, A. A. Reynoso, K. Biermann, P. V. Santos and A. Fainstein, Polariton-driven phonon laser, *Nat. Commun.*, 2020, **11**(1), 4552.
12 H. Jing, S. K. Ozdemir, X. Y. Lü, J. Zhang, L. Yang and F. Nori, PT-symmetric phonon laser, *Phys. Rev. Lett.*, 2014, **113**(5), 053604.
13 M. Toroš, U. Delić, F. Hales and T. S. Monteiro, Coherent-scattering two-dimensional cooling in levitated cavity optomechanics, *Phys. Rev. Res.*, 2021, **3**(2), 023071.
14 A. Schliesser, O. Arcizet, R. Rivière, G. Anetsberger and T. J. Kippenberg, Resolved-sideband cooling and position measurement of a micromechanical oscillator close to the Heisenberg uncertainty limit, *Nat. Phys.*, 2009, **5**(7), 509–514.
15 Y. S. Park and H. Wang, Resolved-sideband and cryogenic cooling of an optomechanical resonator, *Nat. Phys.*, 2009, **5**(7), 489–493.
16 A. Schliesser, P. Del'Haye, N. Nooshi, K. J. Vahala and T. J. Kippenberg, Radiation pressure cooling of a micromechanical oscillator using dynamical backaction, *Phys. Rev. Lett.*, 2006, **97**(24), 243905.
17 D. Kleckner and D. Bouwmeester, Sub-kelvin optical cooling of a micromechanical resonator, *Nature*, 2006, **444**(7115), 75–78.
18 H. Xu, L. Jiang, A. A. Clerk and J. G. E. Harris, Nonreciprocal control and cooling of phonon modes in an optomechanical system, *Nature*, 2019, **568**(7750), 65–69.
19 N. T. Otterstrom, R. O. Behunin, E. A. Kittlaus and P. T. Rakich, Optomechanical cooling in a continuous system, *Phys. Rev. X*, 2018, **8**(4), 041034.
20 D. G. Lai, F. Zou, B. P. Hou, Y. F. Xiao and J. Q. Liao, Simultaneous cooling of coupled mechanical resonators in cavity optomechanics, *Phys. Rev. A*, 2018, **98**(2), 023860.
21 N. Fiaschi, B. Hensen, A. Wallucks, R. Benevides, J. Li, T. P. M. Alegre and S. Gröblacher, Optomechanical quantum teleportation, *Nat. Photonics*, 2021, **15**(11), 817–821.
22 S. Barzanjeh, A. Xuereb, S. Gröblacher, M. Paternostro, C. A. Regal and E. M. Weig, Optomechanics for quantum technologies, *Nat. Phys.*, 2021, **18**(1), 15–24.
23 R. Riedinger, A. Wallucks, I. Marinkovic, C. Loschnauer, M. Aspelmeyer, S. Hong and S. Groblacher, Remote quantum entanglement between two micromechanical oscillators, *Nature*, 2018, **556**(7702), 473–477.
24 M. Metcalfe, Applications of cavity optomechanics, *Appl. Phys. Rev.*, 2014, **1**(3), 031105.
25 Q. Q. Wang, Y. Zheng, C. H. Zhai, X. D. Li, Q. H. Gong and J. Wang, Chip-based quantum communications, *J. Semicond.*, 2021, **42**(9), 091901.

26 Y. Chen, S. L. Li, X. J. Shang, X. B. Su, H. M. Hao, J. X. Shen, Y. Zhang, H. Q. Ni, Y. Ding and Z. C. Niu, Fiber coupled high count-rate single-photon generated from InAs quantum dots, *J. Semicond.*, 2021, **42**, 072901.
27 M. Toroš and T. S. Monteiro, Quantum sensing and cooling in three-dimensional levitated cavity optomechanics, *Phys. Rev. Res.*, 2020, **2**(2), 023228.
28 T. D. Stowe, K. Yasumura, T. W. Kenny, D. Botkin, K. Wago and D. Rugar, Attonewton force detection using ultrathin silicon cantilevers, *Appl. Phys. Lett.*, 1997, **71**(2), 288–290.
29 J. T. Santos, J. Li, J. Ilves, C. F. Ockeloen-Korppi and M. Sillanpää, Optomechanical measurement of a millimeter-sized mechanical oscillator approaching the quantum ground state, *New J. Phys.*, 2017, **19**(10), 103014.
30 L. B. Andre, L. Cheng and S. C. Rand, Saturation, allowed transitions and quantum interference in laser cooling of solids, *Appl. Sci.*, 2022, **12**(3), 953.
31 L. Magrini, P. Rosenzweig, C. Bach, A. Deutschmann-Olek, S. G. Hofer, S. Hong, N. Kiesel, A. Kugi and M. Aspelmeyer, Real-time optimal quantum control of mechanical motion at room temperature, *Nature*, 2021, **595**(7867), 373–377.
32 I. Yeo, H. J. Kim, J. D. Song and K. S. Yi, Hybrid quantum optomechanics with a quantum-dot single photon source, *Phys. Rev. B*, 2016, **94**(16), 165422.
33 R. Weiss, Nobel Lecture: LIGO and the discovery of gravitational waves I, *Rev. Mod. Phys.*, 2018, **90**(4), 040501.
34 D. W. Zhang, C. You and X. Y. Lü, Intermittent chaos in cavity optomechanics, *Phys. Rev. A*, 2020, **101**(5), 053851.
35 X. Y. Lü, H. Jing, J. Y. Ma and Y. Wu, PT-symmetry-breaking chaos in optomechanics, *Phys. Rev. Lett.*, 2015, **114**(25), 253601.
36 J. Zhang, B. Peng, S. Kim, F. Monifi, X. Jiang, Y. Li, P. Yu, L. Liu, Y. X. Liu, A. Alu and L. Yang, Optomechanical dissipative solitons, *Nature*, 2021, **600**(7887), 75–80.
37 A. Ganesan, C. Do and A. Seshia, Phononic frequency comb via intrinsic three-wave mixing, *Phys. Rev. Lett.*, 2017, **118**(3), 033903.
38 M. A. Miri, G. D'Aguanno and A. Alù, Optomechanical frequency combs, *New J. Phys.*, 2018, **20**(4), 043013.
39 M. J. Woolley and A. A. Clerk, Two-mode squeezed states in cavity optomechanics via engineering of a single reservoir, *Phys. Rev. A*, 2014, **89**(6), 063805.
40 M. Montinaro, G. Wust, M. Munsch, Y. Fontana, E. Russo-Averchi, M. Heiss, I. M. A. Fontcuberta, R. J. Warburton and M. Poggio, Quantum dot opto-mechanics in a fully self-assembled nanowire, *Nano Lett.*, 2014, **14**(8), 4454–4460.
41 I. Yeo, P. L. de Assis, A. Gloppe, E. Dupont-Ferrier, P. Verlot, N. S. Malik, E. Dupuy, J. Claudon, J. M. Gerard, A. Auffeves, G. Nogues, S. Seidelin, J. P. Poizat, O. Arcizet and M. Richard, Strain-mediated coupling in a quantum dot-mechanical oscillator hybrid system, *Nat. Nanotechnol.*, 2014, **9**(2), 106–110.
42 H. Okamoto, T. Watanabe, R. Ohta, K. Onomitsu, H. Gotoh, T. Sogawa and H. Yamaguchi, Cavity-less on-chip optomechanics using excitonic transitions in semiconductor heterostructures, *Nat. Commun.*, 2015, **6**, 8478.
43 H. Okamoto, D. Ito, K. Onomitsu, H. Sanada, H. Gotoh, T. Sogawa and H. Yamaguchi, Vibration amplification, damping, and self-oscillations in micromechanical resonators induced by optomechanical coupling through carrier excitation, *Phys. Rev. Lett.*, 2011, **106**(3), 036801.
44 J. Zhang, Q. Zhang, X. Wang, L. C. Kwek and Q. Xiong, Resolved-sideband Raman cooling of an optical phonon in semiconductor materials, *Nat. Photonics*, 2016, **10**(9), 600–605.
45 H. Xie, S. Jiang, D. A. Rhodes, J. C. Hone, J. Shan and K. F. Mak, Tunable exciton-optomechanical coupling in suspended monolayer $MoSe_2$, *Nano Lett.*, 2021, **21**(6), 2538–2543.
46 J. M. Lai, Y. R. Xie and J. Zhang, Detection of electron-phonon coupling in two-dimensional materials by light scattering, *Nano Res.*, 2020, **14**(6), 1711–1733.
47 Y. F. Gao, J. M. Lai and J. Zhang, Optical control of bulk phonon modes in crystalline solids, *Adv. Quantum Technol.*, 2021, **5**(2), 2100103.
48 P. N. Lebedev, Untersuchungen über die Druckkräfte des Lichtes, *Ann. Phys.*, 1901, **311**, 433–458.
49 V. R. Friseh, Experimenteller nachweis des Einsteinschen strahlungsrückstoßes, *Z. Phys.*, 1933, **86**, 42–48.
50 R. A. Beth, Mechanical detection and measurement of the angular momentum of light, *Phys. Rev.*, 1936, **50**(2), 115–125.
51 J. Chan, T. P. Alegre, A. H. Safavi-Naeini, J. T. Hill, A. Krause, S. Groblacher, M. Aspelmeyer and O. Painter, Laser cooling of a nanomechanical oscillator into its quantum ground state, *Nature*, 2011, **478**(7367), 89–92.
52 M. J. Weaver, F. Buters, F. Luna, H. Eerkens, K. Heeck, S. de Man and D. Bouwmeester, Coherent optomechanical state transfer between disparate mechanical resonators, *Nat. Commun.*, 2017, **8**(1), 824.
53 X. Jiang and L. Yang, Optothermal dynamics in whispering-gallery microresonators, *Light: Sci. Appl.*, 2020, **9**, 24.
54 J. Gargiulo, T. Brick, I. L. Violi, F. C. Herrera, T. Shibanuma, P. Albella, F. G. Requejo, E. Cortes, S. A. Maier and F. D. Stefani, Understanding and reducing photothermal forces for the fabrication of Au nanoparticle dimers by optical printing, *Nano Lett.*, 2017, **17**(9), 5747–5755.
55 A. G. Primo, C. M. Kersul, R. Benevides, N. C. Carvalho, M. Ménard, N. C. Frateschi, P. L. de Assis, G. S. Wiederhecker and T. P. Mayer Alegre, Accurate modeling and characterization of photothermal forces in optomechanics, *APL Photonics*, 2021, **6**(8), 086101.
56 P. Snapp, P. Kang, J. Leem and S. Nam, Colloidal photonic crystal strain sensor integrated with deformable graphene phototransducer, *Adv. Funct. Mater.*, 2019, **29**(33), 1902216.
57 J. S. Bunch, A. M. van der Zande, S. S. Verbridge, I. W. Frank, D. M. Tanenbaum, J. M. Parpia, H. G. Craighead and P. L. McEuen, Electromechanical

resonators from graphene sheets, *Science*, 2007, **315**(5811), 490–493.
58 V. Singh, S. J. Bosman, B. H. Schneider, Y. M. Blanter, A. Castellanos-Gomez and G. A. Steele, Optomechanical coupling between a multilayer graphene mechanical resonator and a superconducting microwave cavity, *Nat. Nanotechnol.*, 2014, **9**(10), 820–824.
59 C. Chen, S. Rosenblatt, K. I. Bolotin, W. Kalb, P. Kim, I. Kymissis, H. L. Stormer, T. F. Heinz and J. Hone, Performance of monolayer graphene nanomechanical resonators with electrical readout, *Nat. Nanotechnol.*, 2009, **4**(12), 861–867.
60 V. Singh, S. Sengupta, H. S. Solanki, R. Dhall, A. Allain, S. Dhara, P. Pant and M. M. Deshmukh, Probing thermal expansion of graphene and modal dispersion at low-temperature using graphene nanoelectromechanical systems resonators, *Nanotechnology*, 2010, **21**(16), 165204.
61 R. De Alba, F. Massel, I. R. Storch, T. S. Abhilash, A. Hui, P. L. McEuen, H. G. Craighead and J. M. Parpia, Tunable phonon-cavity coupling in graphene membranes, *Nat. Nanotechnol.*, 2016, **11**(9), 741–746.
62 S. L. Ren, Q. H. Tan and J. Zhang, Review on the quantum emitters in two-dimensional materials, *J. Semicond.*, 2019, **40**(7), 071903.
63 C. Lee, X. Wei, J. W. Kysar and J. Hone, Measurement of the elastic properties and intrinsic strength of monolayer graphene, *Science*, 2008, **321**(5887), 385–388.
64 P. Weber, J. Guttinger, A. Noury, J. Vergara-Cruz and A. Bachtold, Force sensitivity of multilayer graphene optomechanical devices, *Nat. Commun.*, 2016, **7**, 12496.
65 X. Song, M. Oksanen, J. Li, P. J. Hakonen and M. A. Sillanpaa, Graphene optomechanics realized at microwave frequencies, *Phys. Rev. Lett.*, 2014, **113**(2), 027404.
66 B. Yao, C. Yu, Y. Wu, S. W. Huang, H. Wu, Y. Gong, Y. Chen, Y. Li, C. W. Wong, X. Fan and Y. Rao, Graphene-enhanced Brillouin optomechanical microresonator for ultrasensitive gas detection, *Nano Lett.*, 2017, **17**(8), 4996–5002.
67 G. Fugallo, A. Cepellotti, L. Paulatto, M. Lazzeri, N. Marzari and F. Mauri, Thermal conductivity of graphene and graphite: collective excitations and mean free paths, *Nano Lett.*, 2014, **14**(11), 6109–6114.
68 J. Zhu, Q. H. Liu and T. Lin, Manipulating light absorption of graphene using plasmonic nanoparticles, *Nanoscale*, 2013, **5**(17), 7785–7789.
69 J. Lee, M. D. LaHaye and P. X. L. Feng, Design of strongly nonlinear graphene nanoelectromechanical systems in quantum regime, *Appl. Phys. Lett.*, 2022, **120**(1), 014001.
70 R. A. Barton, I. R. Storch, V. P. Adiga, R. Sakakibara, B. R. Cipriany, B. Ilic, S. P. Wang, P. Ong, P. L. McEuen, J. M. Parpia and H. G. Craighead, Photothermal self-oscillation and laser cooling of graphene optomechanical systems, *Nano Lett.*, 2012, **12**(9), 4681–4686.
71 R. Singh, R. J. T. Nicholl, K. I. Bolotin and S. Ghosh, Motion transduction with thermo-mechanically squeezed graphene resonator modes, *Nano Lett.*, 2018, **18**(11), 6719–6724.
72 Y. Xiao, F. Luo, Y. Zhang, F. Hu, M. Zhu and S. Qin, A Review on graphene-based nano-electromechanical resonators: fabrication, performance, and applications, *Micromachines*, 2022, **13**(2), 215.
73 N. I. Landy, S. Sajuyigbe, J. J. Mock, D. R. Smith and W. J. Padilla, Perfect metamaterial absorber, *Phys. Rev. Lett.*, 2008, **100**(20), 207402.
74 T. Paul, C. Menzel, C. Rockstuhl and F. Lederer, Advanced optical metamaterials, *Adv. Mater.*, 2010, **22**(21), 2354–2357.
75 K. L. Tsakmakidis, A. D. Boardman and O. Hess, 'Trapped rainbow' storage of light in metamaterials, *Nature*, 2007, **450**(7168), 397–401.
76 X. Xie, S. S. Shi and X. L. Xu, Coupling between quantum dots and photonic nanostructures, *J. Semicond.*, 2020, **41**(6), 060401.
77 H. Zhu, F. Yi and E. Cubukcu, Plasmonic metamaterial absorber for broadband manipulation of mechanical resonances, *Nat. Photonics*, 2016, **10**(11), 709–714.
78 P. Ruello, Photothermal optomechanics, *Nat. Photonics*, 2016, **10**(11), 692–693.
79 M. Esmann, F. R. Lamberti, A. Harouri, L. Lanco, I. Sagnes, I. Favero, G. Aubin, C. Gomez-Carbonell, A. Lemaître, O. Krebs, P. Senellart and N. D. Lanzillotti-Kimura, Brillouin scattering in hybrid optophononic Bragg micropillar resonators at 300 GHz, *Optica*, 2019, **6**(7), 854–859.
80 S. Anguiano, A. E. Bruchhausen, B. Jusserand, I. Favero, F. R. Lamberti, L. Lanco, I. Sagnes, A. Lemaitre, N. D. Lanzillotti-Kimura, P. Senellart and A. Fainstein, Micropillar resonators for optomechanics in the extremely high 19–95-GHz frequency range, *Phys. Rev. Lett.*, 2017, **118**(26), 263901.
81 A. Fainstein, B. Jusserand and V. Thierry-Mieg, Raman scattering enhancement by optical confinement in a semiconductor planar microcavity, *Phys. Rev. Lett.*, 1995, **75**(20), 3764–3767.
82 P. Y. Yu and M. Cardona, Optical Properties I, in *Fundamentals of Semiconductors*, Graduate Texts in Physics, Springer, Berlin, Heidelberg, 2010.
83 M. Eichenfield, C. P. Michael, R. Perahia and O. Painter, Actuation of micro-optomechanical systems via cavity-enhanced optical dipole forces, *Nat. Photonics*, 2007, **1**(7), 416–422.
84 G. Bahl and T. Carmon, Brillouin Optomechanics, in *Cavity Optomechanics*, Quantum Science and Technology, Springer, Berlin, Heidelberg, 2014.
85 A. Baydin, H. Krzyzanowska, R. Gatamov, J. Garnett and N. Tolk, The photoelastic coefficient P12 of H(+) implanted GaAs as a function of defect density, *Sci. Rep.*, 2017, **7**(1), 15150.
86 W. Primak and D. Post, Photoelastic constants of vitreous silica and its elastic coefficient of refractive index, *J. Appl. Phys.*, 1959, **30**(5), 779–788.

87 N. D. Lanzillotti-Kimura, A. Fainstein, B. Perrin, B. Jusserand, O. Mauguin, L. Largeau and A. Lemaitre, Bloch oscillations of THz acoustic phonons in coupled nanocavity structures, *Phys. Rev. Lett.*, 2010, **104**(19), 197402.

88 G. Rozas, M. F. Winter, B. Jusserand, A. Fainstein, B. Perrin, E. Semenova and A. Lemaitre, Lifetime of THz acoustic nanocavity modes, *Phys. Rev. Lett.*, 2009, **102**(1), 015502.

89 A. Fainstein, A. N, D. Lanzillotti-Kimura, B. Jusserand and B. Perrin, Strong optical-mechanical coupling in a vertical GaAs/AlAs microcavity for subterahertz phonons and near-infrared light, *Phys. Rev. Lett.*, 2013, **110**(3), 037403.

90 P. Roelli, C. Galland, N. Piro and T. J. Kippenberg, Molecular cavity optomechanics as a theory of plasmon-enhanced Raman scattering, *Nat. Nanotechnol.*, 2016, **11**(2), 164–169.

91 S. M. Ashrafi, R. Malekfar, A. R. Bahrampour and J. Feist, Optomechanical heat transfer between molecules in a nanoplasmonic cavity, *Phys. Rev. A*, 2019, **100**(1), 013826.

92 W. L. Barnes, A. Dereux and T. W. Ebbesen, Surface plasmon subwavelength optics, *Nature*, 2003, **424**, 824–830.

93 M. S. Tame, K. R. McEnery, S. K. Özdemir, J. Lee, S. A. Maier and M. S. Kim, Quantum plasmonics, *Nat. Phys.*, 2013, **9**(6), 329–340.

94 M. Fleischmann, P. Hendra and A. J. McQuillan, Raman spectra of pyridine adsorbed at a silver electrode, *Chem. Phys. Lett.*, 1974, **26**, 163–166.

95 M. K. Schmidt and J. Aizpurua, Nanocavities: Optomechanics goes molecular, *Nat. Nanotechnol.*, 2016, **11**(2), 114–115.

96 F. Benz, M. K. Schmidt, A. Dreismann, R. Chikkaraddy, Y. Zhang, A. Demetriadou, C. Carnegie, H. Ohadi, B. Nijs, R. Esteban, J. Aizpurua and J. J. Baumberg, Single-molecule optomechanics in "picocavities", *Science*, 2016, **354**, 726–729.

97 K. Kneipp, Y. Wang, H. Kneipp, L. T. Perelman, I. Itzkan, R. R. Dasari and M. S. Feld, Single molecule detection using surface-enhanced Raman scattering (SERS), *Phys. Rev. Lett.*, 1997, **78**(9), 1667–1670.

98 M. K. Schmidt, R. Esteban, A. Gonzalez-Tudela, G. Giedke and J. Aizpurua, Quantum mechanical description of Raman scattering from molecules in plasmonic cavities, *ACS Nano*, 2016, **10**(6), 6291–6298.

99 S. M. Nie and S. R. Emory, Probing single molecules and single nanoparticles by surface-enhanced Raman scattering, *Science*, 1997, **275**, 1102–1106.

100 J. Feng, J. Wang, A. Fieramosca, R. Bao, J. Zhao, R. Su, Y. Peng, T. C. H. Liew, D. Sanvitto and Q. H. Xiong, All-optical switching based on interacting exciton polaritons in self-assembled perovskite microwires, *Sci. Adv.*, 2021, **7**(46), eabj6627.

101 A. Barg, L. Midolo, G. Kiršanske, P. Tighineanu, T. Pregnolato, A. Imamoglu, P. Lodahl, A. Schliesser, S. Stobbe and E. S. Polzik, Carrier-mediated optomechanical forces in semiconductor nanomembranes with coupled quantum wells, *Phys. Rev. B: Condens. Matter Mater. Phys.*, 2011, **98**, 155316.

102 M. Cardona and N. E. Christensen, Acoustic deformation potentials and heterostructure band offsets in semiconductors, *Phys. Rev. B: Condens. Matter Mater. Phys.*, 1987, **35**(12), 6182–6194.

103 H. J. Conley, B. Wang, J. I. Ziegler, R. F. J. Haglund, S. T. Pantelides and K. I. Bolotin, Bandgap engineering of strained monolayer and bilayer MoS_2, *Nano Lett.*, 2013, **13**(8), 3626–3630.

104 W. Ibarra-Hernández, A. C. Garcia-Castro, A. Bautista-Hernández, M. Salazar-Villanueva, A. Cantarero and A. H. Romero, Modification of electronic and thermoelectric properties of InSe/GaSe superlattices by strain engineering, *Phys. Rev. Mater.*, 2022, **6**(2), 025403.

105 R. Frisenda, M. Drüppel, R. Schmidt, S. M. Vasconcellos, D. P. Lara, R. Bratschitsch, M. Rohlfing and A. Castellanos-Gomez, Biaxial strain tuning of the optical properties of single-layer transition metal dichalcogenides, *npj 2D Mater. Appl.*, 2017, **1**(1), 1–7.

106 F. Miao, S. J. Liang and B. Cheng, Straintronics with van der Waals materials, *npj Quantum Mater.*, 2021, **6**(1), 1–4.

107 P. Chen, T. L. Atallah, Z. Lin, P. Wang, S. J. Lee, J. Xu, Z. Huang, X. Duan, Y. Ping, Y. Huang, J. R. Caram and X. Duan, Approaching the intrinsic exciton physics limit in two-dimensional semiconductor diodes, *Nature*, 2021, **599**(7885), 404–410.

108 G. D. Schiles and G. Rumbles, Excitons in nanoscale systems, *Nat. Mater.*, 2006, **5**, 683–696.

109 Z. Peng, X. Chen, Y. Fan, D. J. Srolovitz and D. Lei, Strain engineering of 2D semiconductors and graphene from strain fields to band-structure tuning and photonic applications, *Light: Sci. Appl.*, 2020, **9**, 190.

110 K. He, C. Poole, K. F. Mak and J. Shan, Experimental demonstration of continuous electronic structure tuning via strain in atomically thin MoS_2, *Nano Lett.*, 2013, **13**(6), 2931–2936.

111 Z. Shuai, L. Wang and C. Song, Deformation potential theory, in *Theory of charge transport in carbon electronic materials*, 2012, pp. 67–88.

112 S. Bertolazzi, J. Brivio and A. Kis, Stretching and breaking of ultrathin MoS_2, *ACS Nano*, 2011, **5**(12), 9703–9709.

113 J. Lee, Z. Wang, K. He, R. Yang, J. Shan and P. X.-L. Feng, Electrically tunable single- and few-layer MoS_2 nanoelectromechanical systems with broad dynamic range, *Sci. Adv.*, 2018, **4**, eaao6653.

114 A. Eichler, J. Moser, J. Chaste, M. Zdrojek, I. Wilson-Rae and A. Bachtold, Nonlinear damping in mechanical resonators made from carbon nanotubes and graphene, *Nat. Nanotechnol.*, 2011, **6**(6), 339–342.

115 Q. Zhang and J. Zhang, All-optical switching based on self-assembled halide perovskite microwires, *J. Semicond.*, 2022, **43**(1), 010401.

116 E. F. Nichols and G. F. Hull, A preliminary communication on the pressure of heat and light radiation, *Phys. Rev. (Series I)*, 1901, **13**(5), 307–320.

117 E. Gil-Santos, J. J. Ruz, O. Malvar, I. Favero, A. Lemaître, P. M. Kosaka, S. García-López, M. Calleja and J. Tamayo, Optomechanical detection of vibration modes of a single bacterium, *Nat. Nanotechnol.*, 2015, **15**, 469–474.

118 M. Kobecki, A. V. Scherbakov, S. M. Kukhtaruk, D. D. Yaremkevich, T. Henksmeier, A. Trapp, D. Reuter, V. E. Gusev, A. V. Akimov and M. Bayer, Giant photoelasticity of polaritons for detection of coherent phonons in a superlattice with quantum sensitivity, *Phys. Rev. Lett.*, 2022, **128**, 157401.

119 A. Huynh, B. Perrin, N. D. Lanzillotti-Kimura, B. Jusserand, A. Fainstein and A. Lemaître, Subterahertz monochromatic acoustic wave propagation using semiconductor superlattices as transducers, *Phys. Rev. B: Condens. Matter Mater. Phys.*, 2008, **78**, 233302.

120 A. V. Scherbakov, M. Bombeck, J. V. Jäger, A. S. Salasyuk, T. L. Linnik, V. E. Gusev, D. R. Yakovlev, A. V. Akimov and M. Bayer, Picosecond opto-acoustic interferometry and polarimetry in high-index GaAs, *Opt. Express*, 2013, **21**, 16473.

121 A. Bienfait, K. J. Satzinger, Y. P. Zhong, H.-S. Chang, M.-H. Chou, C. R. Conner, É. Dumur, J. Grebel, G. A. Peairs, R. G. Povey and A. N. Cleland, Phonon-mediated quantum state transfer and remote qubit entanglement, *Science*, 2019, **364**, 368.

122 C. M. Reinke and I. El-Kady, Phonon-based scalable platform for chip-scale quantum computing, *AIP Adv.*, 2016, **6**, 122002.

123 M.-A. Lemonde, S. Meesala, A. Sipahigil, M. J. A. Schuetz, M. D. Lukin, M. Loncar and P. Rabl, Phonon networks with silicon-vacancy centers in diamond waveguides, *Phys. Rev. Lett.*, 2018, **120**, 213603.

124 A. A. Clerk, K. W. Lehnert, P. Bertet, J. R. Petta and Y. Nakamura, Hybrid quantum systems with circuit quantum electrodynamics, *Nat. Phys.*, 2020, **16**, 257.

125 W. H. Renninger, P. Kharel, R. O. Behunin and P. T. Rakich, Bulk crystalline optomechanics, *Nat. Phys.*, 2018, **14**, 601.

126 K. J. Satzinger, Y. P. Zhong, H.-S. Chang, G. A. Peairs, A. Bienfait, M.-H. Chou, A. Y. Cleland, C. R. Conner, É. Dumur, J. Grebel, I. Gutierrez, B. H. November, R. G. Povey, S. J. Whiteley, D. D. Awschalom, D. I. Schuster and A. N. Cleland, Quantum control of surface acoustic-wave phonons, *Nature*, 2018, **563**, 661.

127 B. Jusserand, A. N. Poddubny, A. V. Poshakinskiy, A. Fainstein and A. Lemaitre, Polariton resonances for ultrastrong coupling cavity optomechanics in GaAs/AlAs multiple quantum wells, *Phys. Rev. Lett.*, 2015, **115**, 267402.

128 A. S. Kuznetsov, D. H. O. Machado, K. Biermann and P. V. Santos, Electrically driven microcavity exciton-polariton optomechanics at 20 GHz, *Phy. Rev. X*, 2021, **11**, 021020.

129 A. Crespo-Poveda, A. S. Kuznetsov, A. Hernandez-Minguez, A. Tahraoui, K. Biermann and P. V. Santos, GHz guided optomechanics in planar semiconductor microcavities, *Optica*, 2022, **9**, 160–169.

130 V. Villafañe, P. Sesin, P. Soubelet, S. Anguiano, A. E. Bruchhausen, G. Rozas, C. Gomez Carbonell, A. Lemaître and A. Fainstein, Optoelectronic forces with quantum wells for cavity optomechanics in GaAs/AlAs semiconductor microcavities, *Phys. Rev. B*, 2018, **97**, 195306.

131 N. Carlon Zambon, Z. Denis, R. De Oliveira, S. Ravets, C. Ciuti, I. Favero and J. Bloch, Enhanced cavity optomechanics with quantum-well exciton polaritons, arXiv:2202.12094v1.

132 J. B. Khurgin, Feasibility of resonant Raman cooling and radiation balanced lasing in semiconductors, *J. Opt. Soc. Am. B*, 2022, **39**, 338–344.

133 J. M. Lai, Y. J. Sun, Q. H. Tan, P. H. Tan and J. Zhang, Laser cooling of a lattice vibration in van der Waals semiconductor, *Nano Lett.*, 2022, **22**, 7129–7135.

134 H. N. Chang, Z. Y. Li, W. K. Lou, Q. F. Yao, J. M. Lai, B. Liu, H. Q. Ni, Z. C. Niu, K. Chang and J. Zhang, Terahertz cavity optomechanics using topological nanophononic superlattice, *Nanoscale*, 2022, **14**, 13046–13052.

135 S. Ghosh, R. Su, J. X. Zhao, A. Fieramosca, J. Q. Wu, T. F. Li, Q. Zhang, F. Li, Z. H. Chen, T. Liew, D. Sanvitto and Q. H. Xiong, Microcavity exciton polaritons at room temperature, *Photonics Insights*, 2022, **1**, R04.

